OXFORD

SOT | Society of Toxicology
academic.oup.com/toxsci

TOXICOLOGICAL SCIENCES, 186(2), 2022, 269–287

https://doi.org/10.1093/toxsci/kfac012
Advance Access Publication Date: 4 February 2022
Research article

The Effects of Organophosphate Esters Used as Flame Retardants and Plasticizers on Granulosa, Leydig, and Spermatogonial Cells Analyzed Using High-Content Imaging

Xiaotong Wang,* Trang Luu,* Marc A. Beal,† Tara S. Barton-Maclaren,† Bernard Robaire ,*,‡ and Barbara F. Hales *,1

*Department of Pharmacology & Therapeutics, McGill University, Montreal, Quebec H3G 1Y6, Canada, †Existing Substances Risk Assessment Bureau, Healthy Environments and Consumer Safety Branch, Health Canada, Ottawa, Ontario K1A 0K9, Canada, and ‡Department of Obstetrics & Gynecology, McGill University, Montreal, Quebec H3G 1Y6, Canada

[1]To whom correspondence should be addressed at Department of Pharmacology & Therapeutics, McGill University, 3655 Promenade Sir William Osler, Room 110, Montreal, QC H3G1Y6, Canada. E-mail: barbara.hales@mcgill.ca.

ABSTRACT

The replacement of regulated brominated flame retardants and plasticizers with organophosphate esters (OPEs) has led to their pervasive presence in the environment and in biological matrices. Further, there is evidence that exposure to some of these chemicals is associated with reproductive toxicity. Using a high-content imaging approach, we assessed the effects of exposure to 9 OPEs on cells related to reproductive function: KGN human granulosa cells, MA-10 mouse Leydig cells, and C18-4 mouse spermatogonial cells. The effects of OPEs were compared with those of 2,2′,4,4′-tetrabromodiphenyl ether (BDE-47), a legacy brominated flame retardant. Alterations in several important cell features, including cell survival, mitochondrial dynamics, oxidative stress, lysosomes, and lipid droplets, were analyzed. Most of the OPEs tested displayed higher cytotoxicity than BDE-47 in all 3 cell lines. Effects on phenotypic parameters were specific for each cell type. Several OPEs increased total mitochondria, decreased lysosomes, increased the total area of lipid droplets, and induced oxidative stress in KGN cells; these endpoints were differentially affected in MA-10 and C18-4 cells. Alterations in cell phenotypes were highly correlated in the 2 steroidogenic cell lines for a few triaryl OPEs. Potency ranking using 2 complementary approaches, Toxicological Prioritization Index analyses and the lowest benchmark concentration/administered equivalent dose method, revealed that while most of the OPEs tested were more potent than BDE-47, others showed little to no effect. We propose that these approaches serve as lines of evidence in a screening strategy to identify the potential for reproductive and endocrine effects of emerging chemicals and assist in regulatory decision-making.

Key words: endocrine disrupting chemical; alternatives assessment; benchmark concentrations; administered equivalent doses; ToxPi analyses.

Flame retardants are found in a wide range of building materials and consumer products, from furnishings and textiles to electronics (Darnerud *et al.*, 2001; van der Veen and van der de Boer, 2012). Most flame retardants are not covalently bound; thus, they readily leach out from these end-products into the environment, leading to widespread human exposure (Rahman *et al.*, 2001; van der Veen and van der de Boer, 2012). Indeed, flame retardants are frequently detected in environmental media and in a variety of human matrices, such as hair, nails, blood, milk, urine, follicular fluid, and placental tissues (Ding *et al.*, 2016; Harley *et al.*, 2010; Johnson *et al.*, 2012; Kubwabo *et al.*, 2013; Lefèvre *et al.*, 2021; Liu et al., 2015a,b; Ruis *et al.*, 2019; Siddique *et al.*, 2020; Stapleton *et al.*, 2012). Polybrominated diphenyl ethers (PBDEs) were used extensively as flame retardants for decades; 2,2′,4,4′-tetrabromodiphenyl ether (BDE-47) is one of the most abundant PBDE congeners in the environment and in human tissues. However, *in vitro*, *in vivo*, and epidemiological data have provided evidence that PBDEs act as endocrine disrupting chemicals, both in humans and other species, with adverse effects on development and reproduction, the brain, thyroid, and other organs (Allais *et al.*, 2020; Allen *et al.*, 2016; Choi *et al.*, 2019; Darnerud, 2003; Darnerud *et al.*, 2001; Harley *et al.*, 2010; Hoffman *et al.*, 2017; Ingle *et al.*, 2020a,b; Johnson *et al.*, 2012; Lefèvre *et al.*, 2016a; Tung *et al.*, 2016, 2017). Exposure to PBDEs may impair reproductive outcomes through interference with ovarian or testicular functions, disruption of sex hormone homeostasis, and alterations in the activities of nuclear hormone receptors (reviewed by Hales and Robaire, 2020; Wang *et al.*, 2021). Concerns over the exposure and health effects of PBDEs have led to their replacement with alternative flame retardants.

Organophosphate esters (OPEs) were used historically as additives in products such as plasticizers, lubricants, hydraulic fluids, paints, and antifoam agents (Chokwe *et al.*, 2020), and now are used increasingly for their flame-retarding properties. The annual global production of OPEs has increased significantly, in parallel with the phasing-out of PBDEs (Greaves and Letcher, 2017; Hou *et al.*, 2016). Consequently, exposure to OPEs is pervasive, and they are now detected both in the environment and in humans at higher levels than those of PBDEs (Blum *et al.*, 2019; Ding *et al.*, 2016; Leonetti *et al.*, 2016; Liu *et al.*, 2016a; Peng *et al.*, 2020; Percy *et al.*, 2020; Ruis *et al.*, 2019). Nevertheless, the potential health hazards of OPEs are poorly characterized. To address the risks associated with a variety of chemicals, authorities, including the Government of Canada (Canadian Environmental Protection Act), the U.S. Environmental Protection Agency (the Design for the Environment Program), and the European Union (Registration, Evaluation, Authorization and Restriction of Chemicals or REACH legislation) have taken initiatives that have resulted in the identification of hazards associated with exposure to some flame retardants and plasticizers. However, the risk assessments for many OPEs are still underway (European Chemicals Agency [ECHA], 2021a; The Government of Canada, 2021; United States Environmental Protection Agency [U.S. EPA], 2014).

A few studies have indicated that exposure to OPEs may be detrimental to fertility. In women, an increase in the concentrations of OPE metabolites in urine was associated with an increase in the incidence of implantation failure, pregnancy loss, or stillbirth after *in vitro* fertilization (IVF; Carignan *et al.*, 2017); similarly, paternal exposure to OPEs was associated with reduced fertilization rates after IVF procedures (Carignan *et al.*, 2018). In animal models, exposure to several OPEs was reported to adversely affect multiple reproductive parameters (eg, fecundity, litter size, and live birth rate) in mice (Chapin *et al.*, 1988; Gulati *et al*, 1991) and in rats (Carlton *et al.*, 1987; European Chemicals Agency [ECHA], 2010, 2021c; Latendresse *et al.*, 1994b), accompanied by histopathological changes in female and male reproductive tissues.

The endocrine disrupting potential of OPEs is suspected as the possible cause, at least in part, of their adverse effects on fertility. ToxCast/Tox21 data (United States Environmental Protection Agency [U.S. EPA], 2021b) and a study by Kojima *et al.* (2013) have revealed that OPEs interact with a wide variety of nuclear receptors, including those for estrogens, progesterone, androgens, and thyroid hormones. Exposure to tri-*ortho*-cresyl phosphate (TOCP, CAS No. 78-30-8; $\geq$ 100 mg/kg/day for 4 weeks) impaired endocrine homeostasis in female mice (Hu *et al.*, 2019; Wang *et al.*, 2019). OPE-based hydraulic fluids (400 or 1000 mg/kg/day) altered the serum concentrations of multiple hormones in exposed female rats (Kinkead *et al.*, 1992; Latendresse *et al.*, 1995). Exposure to OPEs, such as isopropylated triphenyl phosphate (IPPP) or TOCP (10 or $\geq$ 125 μM) dysregulated steroidogenesis, induced oxidative stress, and enhanced autophagy in mouse Leydig cells *in vitro* (Liu *et al.*, 2016b; Schang *et al.*, 2016). In addition to affecting steroidogenic cells, exposure to TOCP ($\geq$ 250 μM) was also found to decrease the viability of spermatogonial stem cells (Liu et al., 2015a,b). Collectively, these data suggest that OPE exposure may impair reproductive health in both females and males by targeting various types of cells in the reproductive system. Here, we have focused our studies on the effects of OPEs that are detected frequently in a major source of human exposure, house dust (Fan *et al.*, 2014; Kubwabo *et al.*, 2021).

We hypothesize that exposure to OPEs will alter the cellular characteristics of cells derived from reproductive tissues to a greater extent than the legacy PBDE flame retardants. To test this hypothesis, we have characterized the bioactivities of 9 OPEs: triphenyl phosphate (TPHP), tris(methylphenyl) phosphate (TMPP), IPPP, *tert*-butylphenyl diphenyl phosphate (BPDP), tris(2,4-di-*tert*-butylphenyl) phosphate (TDtBPP), 2,4-bis(1,1-dimethylethyl)-phenol phosphate (BDMPP), tris(2-butoxyethyl) phosphate (TBOEP), tris(1,3-dichloro-2-propyl) phosphate (TDCIPP), and tris(1-chloro-2-propyl) phosphate (TCIPP), in 3 cell lines related to the female or male reproductive system: KGN human ovarian granulosa cells, MA-10 mouse Leydig cells, and C18-4 mouse spermatogonial cells. These immortalized cell lines preserve key characteristics of primary cells and are stable in culture. Granulosa cells and Leydig cells are gonadal steroidogenic cells; they are responsible for synthesizing sex hormones and thus are essential for folliculogenesis and spermatogenesis (Knight and Glister, 2006; Smith and Walker, 2014). The spermatogonial cell line will help us to understand the effects of OPEs on male germ cells at an early point in their development. A previous study demonstrated that effects on phenotypic markers in these target cells were useful in screening chemical analogs under consideration as replacements for bisphenol A (Rajkumar *et al.*, 2021). A major PBDE congener, BDE-47, was used as a reference flame retardant throughout this study (Health Canada, 2020; Lefevre *et al.*, 2016b; Sjödin *et al.*, 2019). We combined cell-permeable fluorescent dyes with high-content imaging to assess alterations in multiple phenotypic features of cells after exposure to concentrations that ranged from below those commonly found in the environment to those in toxicity studies. Possible links between these alterations in cell phenotypes were investigated by correlation tests. Further, we used several data analysis approaches to compare the chemical potencies and estimate human-relevant doses; these

methods included benchmark modeling, Toxicological Prioritization Index (ToxPi) analyses, and *in vitro* to *in vivo* extrapolation (IVIVE; Health Canada, 2021; United States Environmental Protection Agency [U.S. EPA], 2012). We propose that these approaches serve to assist in addressing data gaps and identify chemicals that are most likely to be responsible alternatives to the brominated flame retardants.

MATERIALS AND METHODS

Chemicals and reagents. DMEM/F-12 (Dulbecco's Modified Eagle Medium/Nutrient Mixture F-12; with L-glutamine, 15 mM HEPES, no phenol red), DMEM (with 4.5 g/l D-glucose, no phenol red), and collagen I (3 mg/ml, rat tail) were obtained from Gibco BRL (Burlington, Ontario, Canada). Cell-permeable fluorescent dyes (Supplementary Table 1) from Invitrogen were purchased from Thermo Fisher Scientific (Waltham, Massachusetts). Charcoal-stripped fetal bovine serum (FBS), charcoal-stripped horse serum, 1× phosphate-buffered saline (PBS), 10× trypsin/EDTA (2.5% trypsin with 22.1 mM EDTA), 100× sodium pyruvate, 100× MEM nonessential amino acids, and 100× penicillin-streptomycin were purchased from Wisent Bioproducts (Montreal, Quebec, Canada). 10× trypsin/EDTA (0.5% trypsin with 0.2% EDTA) and dimethyl sulfoxide (DMSO) were obtained from Sigma-Aldrich (St Louis, Missouri). Table 1 provides a list of the chemicals tested. BDE-47 (CAS No. 5436-43-1), TPHP (CAS No. 115-86-6), TMPP (CAS No. 1330-78-5), TBOEP (CAS No. 78-51-3), and TDCIPP (CAS No. 13674-87-8) were kindly provided by Dr Nicole Kleinstreuer from the National Toxicology Program Interagency Center for the Evaluation of Alternative Toxicological Methods (NICEATM). IPPP (CAS No. 68937-41-7) and TCIPP (CAS No. 13674-84-5) were gifts from Dr Michael G. Wade (Health Canada, Ottawa, Ontario, Canada). BPDP (CAS No. 56803-37-3) was a gift from Dr Heather M. Stapleton (Duke University, Durham, North Carolina). BDMPP (CAS No. 69284-93-1) was purchased from Caledon Laboratory Chemicals (Georgetown, Ontario, Canada). TDtBPP (CAS No. 95906-11-9) was purchased from Toronto Research Chemicals (Toronto, Ontario, Canada).

Cell cultures. The KGN human ovarian granulosa-like tumor cell line was generously provided by Dr Christopher Price and Dr Bruce Murphy (Université de Montréal, Montreal, Canada); use authorization was provided by Dr Toshihiko Yanase (Fukuoka University, Japan; Nishi *et al.*, 2001). The MA-10 mouse Leydig tumor cell line was a gift from Dr Mario Ascoli (University of Iowa, USA; Ascoli, 1981). The C18-4 spermatogonial cell line was a gift from Dr Marie-Claude Hofmann (MD, Anderson Cancer Center, University of Texas, USA; Hofmann *et al.*, 2005).

KGN cells were cultured in phenol red-free DMEM/F-12 medium supplemented with 10% charcoal-stripped FBS and 0.5% 100× penicillin-streptomycin. MA-10 cells were cultured in phenol-red free DMEM/F-12 medium containing 5% charcoal-stripped FBS, 2.5% charcoal-stripped horse serum, 20 mM HEPES (N-(2-hydroxyethyl)piperazine-N'-(2-ethanesulfonic acid)), and 0.5% 100× penicillin-streptomycin. C18-4 cells were cultured in phenol red-free DMEM medium supplemented with 10% charcoal-stripped FBS, 1% 100× nonessential amino acids, 1 mM sodium pyruvate, 0.5% 100× penicillin-streptomycin. KGN and MA-10 cells were maintained at 37°C, and C18-4 cells were maintained at 34°C. All 3 cell lines were cultured in Corning T-75 cell culture flasks (manufactured from virgin polystyrene) in a humidified atmosphere of 5% CO_2. The culture medium was renewed every 2–3 days.

High-content imaging. KGN cells (6000 cells/well), MA-10 cells (2000 cells/well), and C18-4 cells (2000 cells/well) were seeded in the center 60 wells of black opaque 96-well plates (Perkin Elmer, Waltham, Massachusetts). The plates used for KGN cells were coated with 0.2% collagen 1 to facilitate cell adhesion and distribution. The outer-most layer of wells contained 200 µl of PBS to minimize edge effects. The cells were acclimated for 24 h prior to a 48-h exposure to BDE-47 or an OPE at a wide range of concentrations, spanning 5 orders of magnitude (0.5% DMSO control, 0.001, 0.01, 0.1, 1, 5, 10, 20, 50, and 100 µM). The stock solutions of the compounds were first prepared in DMSO, with 2 exceptions: BDMPP was dissolved in acetone and TDtBPP in chloroform and DMSO. The compounds were further diluted in complete culture medium to the annotated concentrations. The final concentration of solvents in the dilutions was 0.5%. The chloroform concentrations were maintained $< 0.2\%$ since higher concentrations damaged the culture plates; extra DMSO was added to adjust the total vehicle volume to 0.5%.

To determine the effects of exposure on cell phenotypes, cells were stained posttreatment with 4 different combinations of cell-permeable fluorescent dyes for 30 min and were washed once to reduce background staining before image acquisition. The dye combinations were optimized to maximize color output with minimal overlap in their emission and excitation wavelengths. The fluorescent dyes were: Hoechst 33342 (stains nuclei), Calcein-AM (stains cytoplasm and reflects cell viability), CellMask Deep Red (stains plasma membrane), CellROX Deep Red (reflects oxidative stress), MitoTracker Green FM (stains total mitochondria), MitoTracker Red CM-H2XRos (stains active mitochondria), LysoTracker Red DND-99 (stains lysosomes), and Nile Red (stains lipid droplets). All 4 combinations contained Hoechst 33342 to stain nuclei for cell counts and 1 dye (Calcein-AM or CellMask Deep Red) to define the cytoplasmic area. More detailed information on the dye combinations and staining procedure is provided in Supplementary Table 1.

The Operetta High Content Imaging System (Perkin Elmer) with a nonconfocal 40× high-NA objective was used for live-cell imaging (9–12 fields/well). The images that were obtained were analyzed using the Columbus Image Data Storage and Analysis System (Perkin Elmer); a variety of cell features was assessed quantitatively based on the fluorescent signals. The detailed settings of the Columbus image analyses were described previously by Rajkumar *et al.* (2021). The analyses for KGN cells were slightly modified in this study; these parameters are provided in the Supplementary Methods section. Quantification data, with a full concentration range for all parameters for each individual chemical, are also provided in Supplementary Figures 4–14.

Benchmark concentration analyses of high-content imaging data. Benchmark modeling was conducted to derive the phenotype-specific benchmark concentrations (BMCs) of the compounds for potency comparisons. The benchmark response (ie, the predetermined level of change relative to control) was set at 10%, as recommended by the U.S. Environmental Protection Agency (U.S. EPA, 2012). These analyses were done according to the procedures described by Rajkumar *et al.* (2021) with minor modifications. In brief, the absolute values of cell counts (as a proxy for cytotoxicity) following chemical exposures were modeled using PROAST 65.5 software package in R console (v.3.6.2). The concentrations that induced a 10% reduction in nuclear counts were reported with their 90% confidence intervals. Concentrations that induced $> 30\%$ cell death relative to control were excluded in further analyses. The 30% cutoff criterion is

Table 1. List of Flame Retardant Chemicals Tested

Chemical (Acronym)	CAS No.	Structure	Purity (%)	Supplier
2,2′,4,4′-tetrabromodiphenyl ether (BDE-47)	5436-43-1	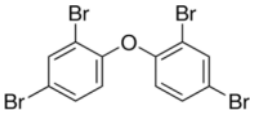	98	Sigma-Aldrich
Triphenyl phosphate (TPHP)	115-86-6	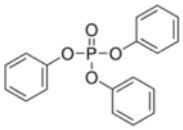	99.9	Sigma-Aldrich
Tris(methylphenyl) phosphate (TMPP)[a]	1330-78-5	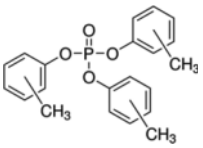	98.6	Sigma-Aldrich
Isopropylated triphenyl phosphate (IPPP)[a]	68937-41-7	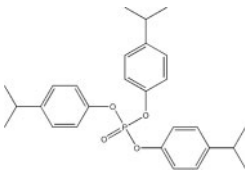	N/A	NIEHS/NTP
tert-Butylphenyl diphenyl phosphate (BPDP)[a]	56803-37-3	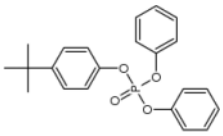	N/A	Scientific Polymer Products
Tris(2,4-di-*tert*-butylphenyl) phosphate (TDtBPP)	95906-11-9	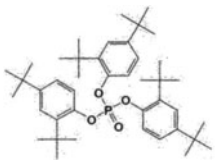	98	Toronto research chemicals
2,4-bis(1,1-dimethylethyl)-phenol phosphate (BDMPP)	69284-93-1	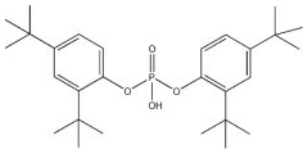	97.3	Caledon laboratory chemicals
Tris(2-butoxyethyl) phosphate (TBOEP)	78-51-3	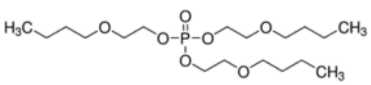	93.6	Sigma-Aldrich
Tris(1,3-dichloro-2-propyl) phosphate (TDCIPP)	13674-87-8	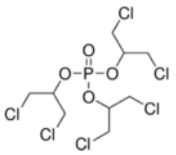	95.9	TCI America
Tris(1-chloro-2-propyl) phosphate (TCIPP)[a]	13674-84-5	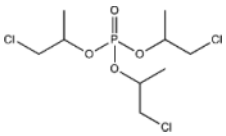	90	AK Scientific

[a]TMPP and TCIPP are isomeric mixtures; IPPP, and BPDP are unspecified mixtures that contain variable amounts of TPHP, and/or mono-, di-, and tri-substitutions.

consistent with other studies using similar approaches (Karmaus *et al.*, 2016; Rajkumar *et al.*, 2021). Data for other phenotypic parameters were first normalized against the controls and were prefiltered with 1-sample *t* tests (ie, compared with 100) in GraphPad Prism (v.8.2.1) with manual Holm-Bonferroni correction; only datasets that showed significant or a trend of differences ($p \leq .05$) and monotonic responses were further analyzed using BMDExpress 2.2 software (SciOne, Research Triangle Park, North Carolina). BMC_{10} values (ie, concentrations with a benchmark response of 10%) were estimated from the best-fit model, based on the lowest Akaike information criterion (AIC); the 95% confidence intervals are reported as BMCL (lower) and BMCU (upper) limits. To ensure the reliability of results, BMCs are only reported if the best-fit model has a global goodness of fit p value $> .1$ and a BMCU/BMCL ratio ≤ 40 (United States Environmental Protection Agency [U.S.EPA], 2012), in addition to the lowest AIC score.

To establish if there are possible relationships among the phenotypic changes that were observed, Spearman's rank correlation tests were done to compute correlation coefficients for every pair of phenotypic parameters using high-content imaging data (normalized). Heatmaps (matrices) of correlation coefficients were generated to compare similarities or differences among the test chemicals.

ToxPi analyses for the potency ranking of the chemicals. The ToxPi software (v.2.3) (available at: https://toxpi.org) was used to rank the chemicals based on their effects on 8 phenotypic endpoints: cytotoxicity, Calcein intensity, oxidative stress, total mitochondria, active mitochondria, number of lysosomes, Lysotracker red intensity, and total area of lipid droplets. The 3 cell lines were analyzed separately. Log_{10}BMC values for all compounds were scaled between 0 and 1 to reflect their relative potencies for each of the 8 endpoints. The least potent compound, ie, no derived BMCs or no effect at the highest concentration tested, was given a score of 0 and the most potent compound (ie, with the lowest endpoint-specific BMC) was given a score of 1. We used base-10 logs to display the range of concentrations over the orders of magnitude and to address skewness towards extreme values. The scaled data were then entered in the required format for importation into the Java-based ToxPi Graphical User Interface (Marvel *et al.*, 2018). Utilizing the input data, the software: (1) calculated compound-specific ToxPi scores using an R-source code for potency ranking (Auerbach *et al.*, 2016); all endpoints were weighted equally in our model (ie, had the same relative emphasis and contributed equally to the calculation); and (2) generated compound-specific ToxPi profiles visualized as pie charts, where each slice represents a single endpoint. The area of each slice is proportional to the relative potency of the compounds for the designated endpoint. The output was used for hierarchical clustering analyses (Ward's D method) using an R-source function (h.clust) built into the ToxPi software. Briefly, each ToxPi profile was initially considered as a single cluster. Then 2 clusters with the highest similarity (ie, the smallest between-cluster distance) were grouped together; this was repeated until all clusters were grouped into one root.

Correlations analyses. Correlations between the lowest BMC rank and the ToxPi rank were assessed using Pearson's tests. The squared Pearson's correlation coefficient (r^2) and the corresponding 2-tailed p values are reported.

In vitro to in vivo extrapolation. IVIVE modeling was conducted to estimate the administered equivalent doses (AEDs, mg/kg body weight/day) based on the BMCs. Analytical details have been provided previously by Rajkumar *et al.* (2021). In brief, the steady-state concentration in the plasma (C_{ss}, with a constant dosing rate of 1 mg/kg body weight/day oral exposure) of each compound was modeled using the high-throughput toxicokinetics (HTTK) package v1.10 in R. Parameters used in IVIVE modeling and the C_{ss} values of the compounds are provided in Supplementary Table 2. Input data were available in HTTK for TPHP and TDCIPP, data for TMPP and TCIPP were available from Health Canada (Health Canada, 2021), and data for BDE-47 were collected following the procedure used by Health Canada (Health Canada, 2021). For the other chemicals lacking *in vitro* parameters of intrinsic clearance and fraction unbound in plasma, *in silico* predictions from ADMET Predictor (version 10) were used in the C_{ss} derivation. BMC values were converted to AEDs using the formula (Health Canada, 2021):

$$\mathrm{AED} = \frac{\mathrm{BMC}\ (\mu\mathrm{M}) \times 1\ \mathrm{mg/kg/day}}{C_{ss}\ (\mu\mathrm{M})}.$$

Statistical analyses. Data are presented as means ± SEM unless otherwise specified. All statistics, curve-fit analyses, and correlation analyses were done using GraphPad Prism (v.8.2.1). Log (inhibitor) versus response (3 parameters) model was used for the nonlinear regression analyses; the lowest response was set as a constant equal to 0. High-content imaging data were normalized against the control value of the same biological replicate; Holm-Bonferroni-corrected 1-sample *t* tests were used to compare the treatment groups with the control. A response with a p value $\leq .05$ and an effect size $\geq 10\%$ was considered to be statistically significant. All experiments were done at least in 2 technical replicates and were repeated independently 6–8 times ($n = 6$–8).

RESULTS

Cytotoxicity of OPEs in KGN, MA-10, and C18-4 Cells

The cytotoxicity of each test chemical was estimated based on the numbers of Hoechst-stained nuclei in the wells. Previously, we reported a good correlation between cell numbers counted by this method and the result of the MTT (3-(4,5-dimethylthiazol-2-yl)-2,5-diphenyltetrazolium bromide) assay which assesses cell metabolic viability (Schang *et al.*, 2016). Nonlinear regression analyses were conducted to calculate the IC_{50} values, ie, the concentrations that induced a 50% reduction in cell counts, for each compound for the 3 cell types (Figure 1). Most of the OPEs exhibited comparable or higher cytotoxicity than BDE-47, with a few exceptions: TDtBPP and TCIPP were not cytotoxic to any of the 3 cell lines and TBOEP was only cytotoxic in MA-10 cells at 100 μM, the highest concentration tested (Supplementary Figure 4). In general, the dose-response curves generated by nonlinear regression analyses for MA-10 cells were steeper than those for KGN or C18-4 cells, demonstrating more sensitivity to the cytotoxicity induced by OPEs; most IC_{50} values were below 20 μM in MA-10 cells. Some chemicals showed cell-specific cytotoxicity. For example, BDMPP showed low cytotoxicity in KGN and C18-4 cells, with an IC_{50} value exceeding the highest concentration tested; however, it was cytotoxic in MA-10 cells, with an IC_{50} of 19.4 μM. Both BDE-47 and TPHP induced low cytotoxicity in KGN cells but exhibited much higher cytotoxicity in the other 2 cell lines. TMPP was the most cytotoxic OPE in both KGN

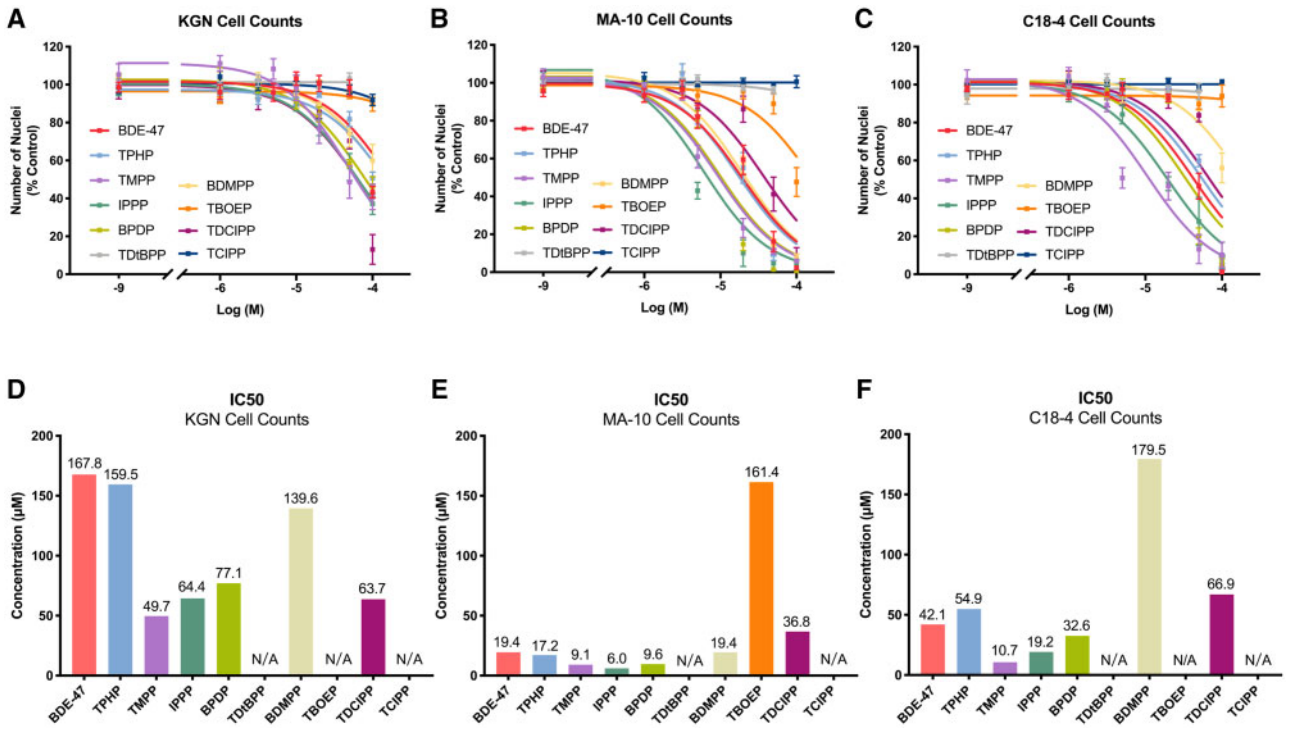

Figure 1. Cytotoxicity of organophosphate esters (OPEs) and 2,2′,4,4′-tetrabromodiphenyl ether (BDE-47) in KGN human granulosa cells (A and D), MA-10 mouse Leydig cells (B and E), C18-4 mouse spermatogonial cells (C and F). Cells were exposed to one of the chemicals for 48 h; numbers of Hoechst 33342 stained nuclei were quantified using Operetta high-content imaging system (40× magnification). Nonlinear regression analyses were conducted to estimate the IC_{50} values of the test chemicals (D–F). Most of the OPEs exhibited similar or higher cytotoxicity than BDE-47 on the 3 cell lines with the exception of tris(2,4-di-*tert*-butylphenyl) phosphate (TDtBPP), tris(2-butoxyethyl) phosphate (TBOEP), and tris(1-chloro-2-propyl) phosphate (TCIPP). Data are shown as percentages relative to controls; values represent means ± SEM; $n = 6–8$. Abbreviation: N/A, not available/applicable.

(IC_{50}: 49.7 μM) and C18-4 cells (IC_{50}: 10.7 μM); IPPP was the most cytotoxic OPE in MA-10 cells (IC_{50}: 6.0 μM; Figure 1).

We also compared the cytotoxicity of each chemical at a threshold response level of 10%. In general, the BMCs associated with a 10% reduction in nuclear counts revealed a similar potency of cytotoxicity as shown by the IC_{50}; however, there were some differences. In KGN cells, TMPP was the OPE with the lowest IC_{50}; however, TDCIPP had the lowest BMC_{10} value (BMC_{10}: 4.4 μM). IPPP had the lowest BMC_{10} in both MA-10 (BMC_{10}: 1.1 μM) and C18-4 cells (BMC_{10}: 12 μM; Supplementary Table 3).

Effects of OPEs on the Phenotypes of KGN, MA-10, and C18-4 Cells

Calcein intensity. The green fluorescence emitted when Calcein-AM is hydrolyzed by an intracellular nonspecific esterase was assessed as a measure of cell viability following exposure to each chemical. It is noteworthy that over 99% of cells that remained in the wells were viable, as determined by positive Calcein staining (Figure 2). A trend towards an increase in Calcein fluorescence was observed only in KGN cells exposed to 20 μM BPDP (Figs. 2A and 2B). However, BDE-47 and 6 OPEs significantly increased the average intensity of Calcein staining in MA-10 cells. Some OPEs induced this increase to a greater extent than BDE-47 (up to 5.6-fold, at the same concentration; Figs. 2C and 2D). The estimated BMCs of the OPEs for effects on Calcein intensity ranged from 0.2 to 11.3 μM in MA-10 cells (Supplementary Table 3); the BMC for BDE-47 for this endpoint was not available due to poor model-fit. Exposure to BPDP (BMC_{10}: 14.4 μM) or TDCIPP (BMC_{10}: 33.5 μM) increased Calcein fluorescence in C18-4 cells while BDE-47 had no effect (Figs. 2E, 2F and Supplementary Table 3).

The production of reactive oxygen species. A change in CellROX intensity (a dye that is nonfluorescent in its reduced form and emits red fluorescence upon oxidation) was used as an indication of oxidative stress. In KGN cells, exposure to TMPP, IPPP, or BPDP significantly increased the intensity of CellROX staining at 20 μM, whereas BDE-47 showed an effect only at 50 μM; effects of exposure to TDCIPP were observed only at 2 middle concentrations (Figs. 3A and 3B).

MA-10 cells were more sensitive to OPE-induced oxidative stress than KGN cells (Figs. 3C and 3D). In total, 6 out of 9 of the OPEs tested increased the intensity of CellROX staining in MA-10 cells; for TPHP this increase was observed at a concentration as low as 0.01 μM (Supplementary Figure 6). The BMCs of OPEs for this endpoint ranged from 3.2 to 46.9 μM (Supplementary Table 3). Interestingly, C18-4 cells had a different response to OPE exposures: TDtBPP (BMC_{10}: 21.1 μM) and BDMPP (BMC_{10}: 16.6 μM) reduced oxidative stress in C18-4 cells, whereas BDE-47 had no effect (Figs. 3E, 3F and Supplementary Table 3).

Mitochondria. A combination of Mitotracker Green and Mitotracker Red dyes was used to assess the effects of OPE exposure on mitochondria. Mitotracker Green accumulates in the mitochondrial matrix regardless of the mitochondrial membrane potential; Mitotracker Red is retained only in active mitochondria. BDE-47 did not affect mitochondrial staining in any of the 3 cell lines (Supplementary Figure 1). In KGN cells, we observed minor but significant increases (approximately 10–30%) in the numbers of both total and active mitochondria after exposure to TMPP (BMC_{10}: 4.6 μM) or BPDP (BMC_{10}: 12.2 μM), albeit the latter parameter did not reach statistical significance (Supplementary Figs. 1A, 1B, 7, and 8 and Supplementary Table 3). However, the ratio of

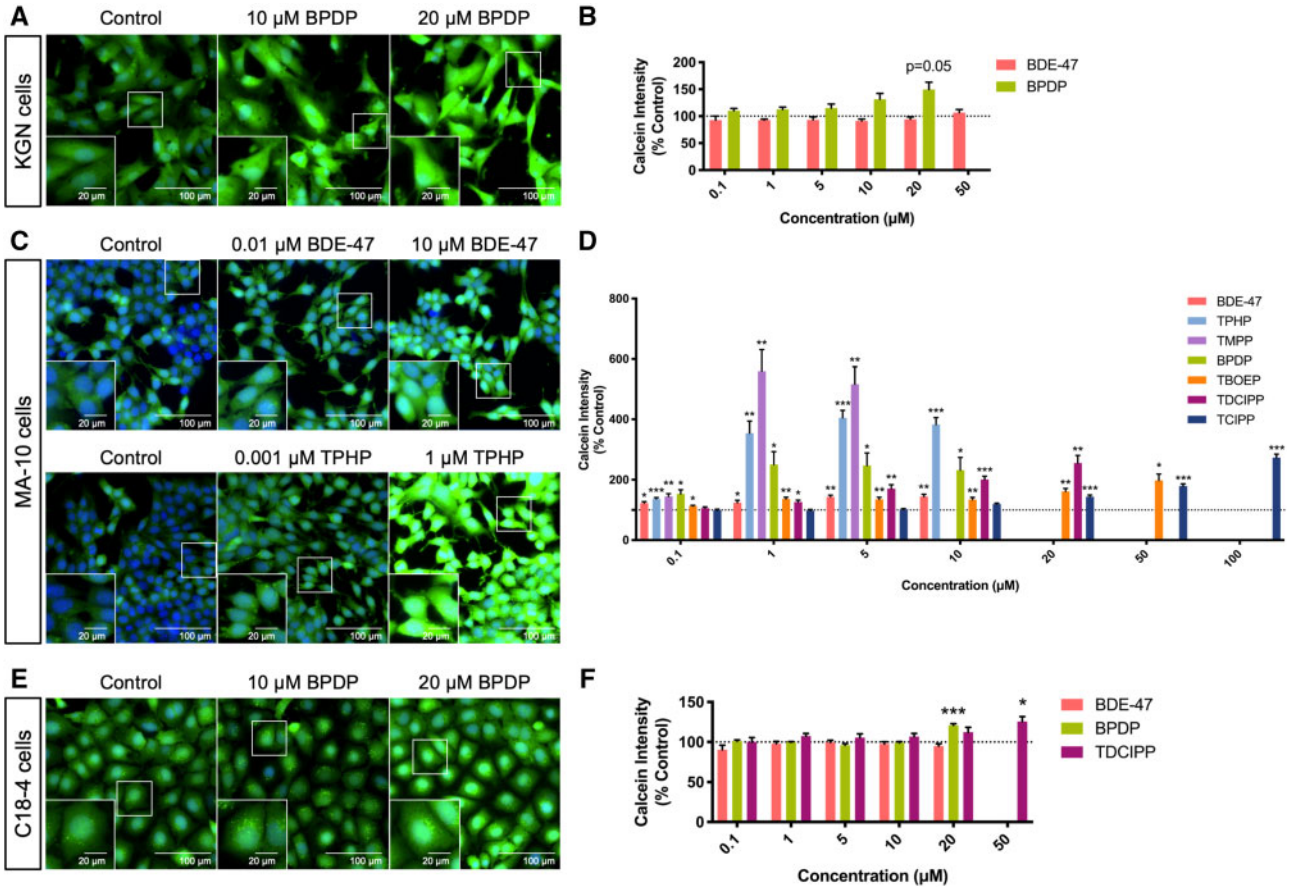

Figure 2. Effects of organophosphate esters (OPEs) and 2,2′,4,4′-tetrabromodiphenyl ether (BDE-47) on Calcein-AM staining intensity in KGN granulosa cells (A and B), MA-10 mouse Leydig cells (C and D), and C18-4 mouse spermatogonial cells (E and F). Cells were stained by Hoechst 33342 (blue, stains nuclei) and Calcein-AM (green, an indicator of cell viability) fluorescent dyes for 30 min and visualized by high-content imaging (40× magnification). Scale bars of the insets and the main images denote 20 and 100 μm, respectively. Bar graphs show the quantification of Calcein-AM staining intensity following 48 h BDE-47 or OPE exposures. Data are shown as percentages relative to controls; values represent means ± SEM; $n = 6–8$. One-sample Holm-Bonferroni-corrected t tests were conducted to determine significant differences from controls (=100): $^{*}p < .05$, $^{**}p < .01$, and $^{***}p < .001$. For ease of visualization, only OPEs with significant findings at one or more treatment concentrations are shown, data for concentrations from 0.1 to 50 or 100 μM are shown. Concentrations that induced > 30% cell death were excluded from the analyses.

active to total mitochondria was not altered in KGN cells by any of the chemicals, suggesting that OPEs may affect the numbers of mitochondria, independently of their activity.

In MA-10 cells, exposure to BPDP (BMC_{10}: 5.6 μM) or TDCIPP (BMC_{10}: 9.1 μM) increased the staining of active mitochondria without affecting total mitochondria (Supplementary Figs. 1C and 1D and Supplementary Table 3). Exposure of these cells to 20 μM of TDCIPP increased the ratio of active to total mitochondria in MA-10 cells (Supplementary Figure 2A).

In C18-4 cells, exposure to TPHP (BMC_{10}: n/a), TMPP (BMC_{10}: 1.4 μM), and TDCIPP (BMC_{10}: 37.1 μM) increased the staining of total mitochondria in the absence of an effect on active mitochondria (Supplementary Figs. 1E, 1F, 7, and 8 and Supplementary Table 3). The proportion of active mitochondria was slightly decreased (approximately 10–15%) in these cells after exposure to TPHP (≥ 1 μM) or BDE-47 (≥ 5 μM; Supplementary Figure 2B).

Lysosomes. The effects of exposure to OPEs on lysosomes in cells were examined using Lysotracker Red, a dye that consists of a fluorophore linked to a weak base that becomes fluorescent once it is protonated in acidic organelles (Chazotte, 2011). Both BDE-47 and some OPEs decreased the average number of lysosomes in KGN cells in a concentration-dependent manner (Figs. 4A and 4B). Exposure to 20 μM BDE-47 induced a 35% decrease in the number of lysosomes, whereas TMPP, the most potent OPE in this cell line, induced a 79% decrease. The BMCs associated with a 10% decrease in the numbers of lysosomes were 5.6 μM for BDE-47, 4.7 μM for TMPP, 13.3 μM for IPPP, and 18.2 μM for BPDP (Supplementary Table 3). Interestingly, BDE-47 (BMC_{10}: 8.0 μM) and TMPP (BMC_{10}: 4.8 μM) both decreased the intensity of Lysotracker Red staining (Supplementary Figure 3); this may be indicative of an increase in lysosomal pH, and thus effects on the activities of lysosomal enzymes. BPDP increased Lysotracker Red intensity by 20–30% at concentrations (0.01 and 0.1 μM,) which were much lower than those required to elicit a reduction in lysosome numbers (Figure 4B and Supplementary Figure 3B). Although BDMPP did not appear to affect the number of lysosomes, it enhanced Lysotracker Red staining by 66% at 50 μM (BMC_{10}: 44.2 μM), suggesting that it may have the ability to impair the function of lysosomes in KGN cells (Supplementary Figs. 3A and 3B).

In MA-10 cells, BDE-47 had no significant effect on either lysosome numbers or Lysotracker Red intensity, whereas some OPEs showed differential effects. Specifically, TDCIPP (BMC_{10}: 12.4 μM) induced a significant increase in the number of lysosomes per cell (Supplementary Table 3). In contrast, TPHP (BMC_{10}: 9.9 μM), BDMPP (BMC_{10}: 0.1 μM), BPDP and TDtBPP induced concentration-dependent decreases (Figs. 4C, 4D, and

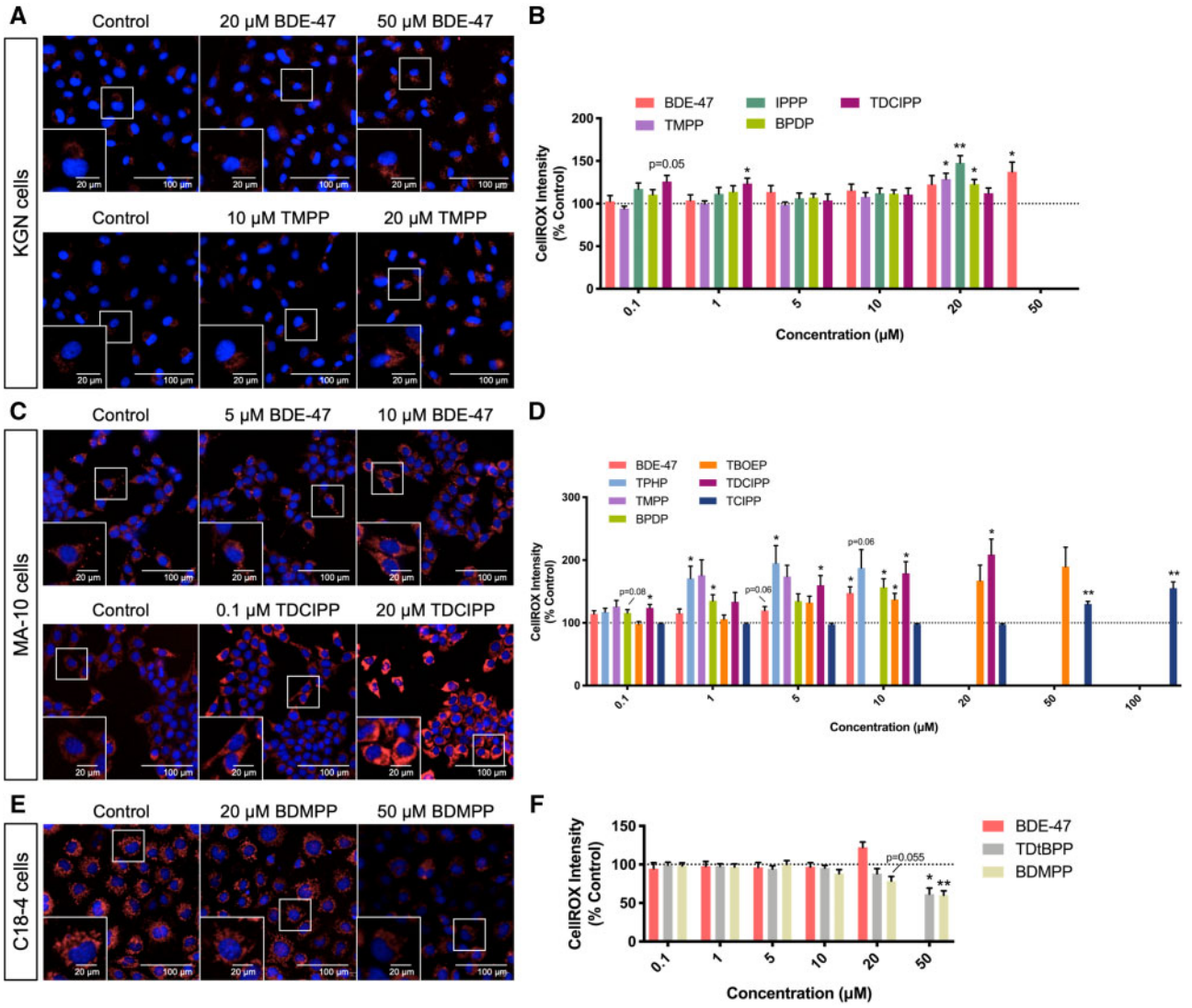

Figure 3. Organophosphate esters (OPEs) and 2,2′,4,4′-tetrabromodiphenyl ether (BDE-47) concentrations with low or no cytotoxicity induced increases in the production of reactive oxygen species in KGN cells (A and B) and MA-10 cells (C and D), while inducing a decrease in C18-4 cells (E and F). Cells were stained by Hoechst 33342 (blue, stains nuclei) and CellROX (red, an indicator of oxidative stress) fluorescent dyes for 30 min and visualized by high-content imaging (40× magnification). Scale bars of the insets and the main images denote 20 and 100 μm, respectively. Bar graphs show the quantification of CellROX staining intensity following 48 h BDE-47 or OPE exposures. Data are shown as percentages relative to controls; values represent means ± SEM; $n = 6$–8. One-sample Holm-Bonferroni-corrected t tests were conducted to determine significant differences from controls (=100): $^{*}p < .05$ and $^{**}p < .01$. For ease of visualization, only OPEs with significant findings at one or more treatment concentrations are shown, with concentrations ranged from 0.1 to 50 or 100 μM. Concentrations that induced > 30% cell death were excluded from the analyses.

Supplementary Table 3); the BMCs for BPDP and TDtBPP were not calculated due to poor model-fits. In addition to its effect on lysosome numbers, BPDP also significantly reduced Lysotracker Red intensity (Supplementary Figs. 3C and 3D). Exposure to TMPP, IPPP, or TBOEP decreased Lysotracker Red intensity to varying degrees, in the absence of effects on lysosome numbers (Supplementary Figure 3D).

In C18-4 cells, BDE-47 did not affect lysosomes. However, BPDP (BMC_{10}: 3.4 μM) decreased the average number of lysosomes in these cells, whereas, IPPP decreased both the number (BMC_{10}: 3.0 μM) and the intensity of Lysotracker Red (BMC_{10}: 4.3 μM); TCIPP exposure increased both the number (BMC_{10}: n/a) and the intensity of lysosome staining (BMC_{10}: 3.6 μM; Figs. 4E, 4F, Supplementary Figs. 3E, 3F, and Supplementary Table 3).

Lipid droplets. Nile Red, a dye that becomes fluorescent in a hydrophobic environment, was used to localize lipid droplets in cells (Greenspan *et al.*, 1985). An increase in the total area of lipid droplets was observed in KGN cells exposed to 50 μM BDE-47. However, much larger increases (approximately 1.3- to 8-fold) in the total area of lipid droplets were observed after exposure to some OPEs at concentrations as low as 1 μM (Figs. 5A and 5B). The BMC for BDE-47 for a 10% increase in lipid droplet areas in KGN cells was 30.8 μM; the BMC_{10} for the most potent OPE, TMPP, was 1.2 μM, whereas the BMC_{10} for the least potent OPE, TBOEP, was 42 μM (Supplementary Table 3).

We observed differential effects of OPEs on lipid droplets in MA-10 and C18-4 cells. Exposure to BDE-47 (at a concentration of 5 μM) or BDMPP (BMC_{10}: 2.6 μM) reduced the total area of lipid droplets in MA-10 cells, whereas 5 μM of IPPP, TDCIPP (BMC_{10}: 9.8 μM), and TCIPP (BMC_{10}: 30.6 μM) slightly but significantly increased the area of lipid droplets (1.1- to 1.3-fold; Figs. 5C, 5D, and Supplementary Table 3).

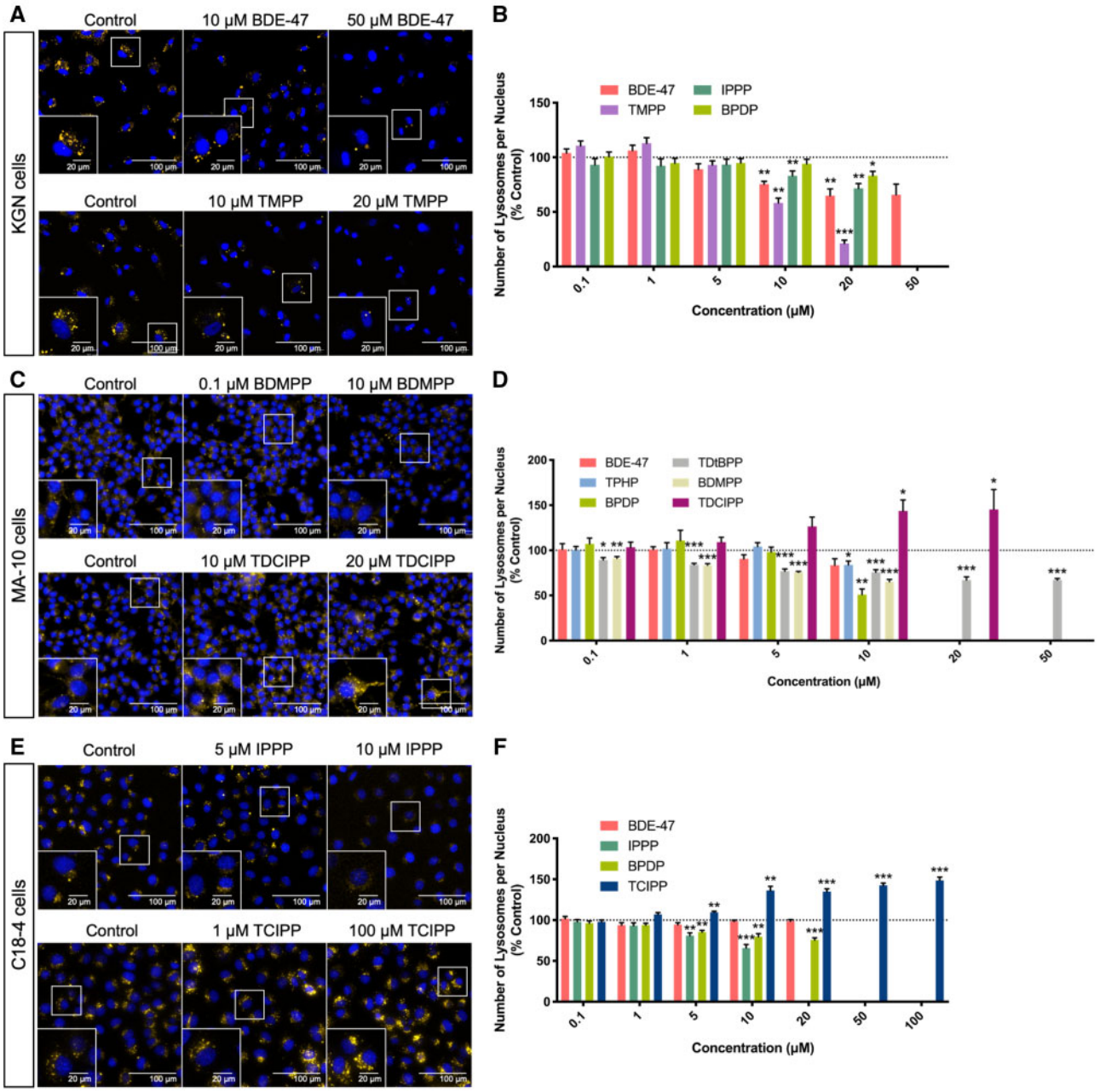

Figure 4. Effects of organophosphate esters (OPEs) and 2,2′,4,4′-tetrabromodiphenyl ether (BDE-47) on the average numbers of lysosomes in KGN cells (A and B), MA-10 cells (C and D), and C18-4 cells (E and F). Cells were stained by Hoechst 33342 (blue, stains nuclei) and Lysotracker Red (yellow, stains lysosomes) fluorescent dyes for 30 min and visualized by high-content imaging (40× magnification). Scale bars of the insets and the main images denote 20 and 100 μm, respectively. Bar graphs show the numbers of lysosomes per nucleus following 48 h BDE-47 or OPE exposures. Data are shown as percentages relative to controls; values represent means ± SEM; $n = 6$–8. One-sample Holm-Bonferroni-corrected t tests were conducted to determine significant differences from controls (=100): $^{*}p < .05$, $^{**}p < .01$, and $^{***}p < .001$. For ease of visualization, only OPEs with significant findings at one or more treatment concentrations are shown, with concentrations ranged from 0.1 to 50 or 100 μM. Concentrations that induced > 30% cell death were excluded from the analyses.

In C18-4 cells, BDMPP (BMC_{10}: 19.1 μM) and TDCIPP (BMC_{10}: 20.4 μM) caused decreases in lipid droplet areas, by 25% and 75%, respectively (Supplementary Table 3). An opposite effect, an increase in lipid droplet areas by up to 40% (Figs. 5E and 5F), was observed after exposure to TPHP (BMC_{10}: 3.6 μM), TDtBPP (BMC_{10}: 18.0 μM), or TCIPP (BMC_{10}: 23.5 μM; Supplementary Table 3). Of note, these changes in the total area of lipid droplets were mainly attributed to the changes in the number of lipid droplets in the cell (Supplementary Figure 14).

Correlations Among Phenotypic Parameters

It is well-established that the functions of many cell organelles are interrelated. We performed Spearman's rank correlation analyses to assess if there was any correlation in our datasets. Concentrations where cell viability was < 90% were excluded. We observed different patterns of correlation heatmaps when comparing chemicals across cell lines (Supplementary Figure 15). Some triaryl OPEs (TMPP, IPPP, and BPDP) showed moderate to strong correlations for their effects on cell phenotypes and

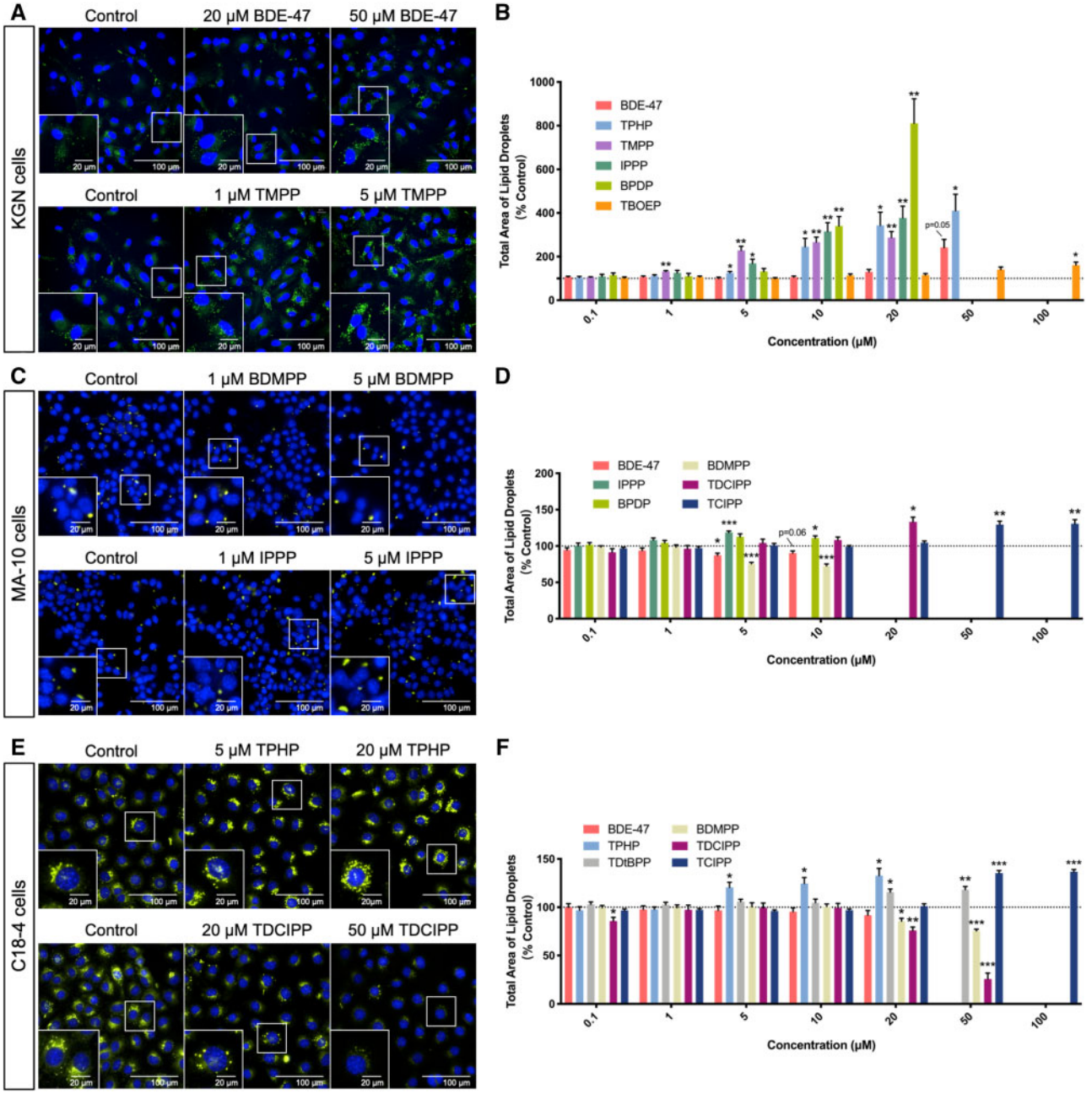

Figure 5. Effects of organophosphate esters (OPEs) and 2,2′,4,4′-tetrabromodiphenyl ether (BDE-47) on lipid homeostasis in KGN cells (A and B), MA-10 cells (C and D), and C18-4 cells (E and F). Nuclei and lipid droplets in cells were stained by Hoechst 33342 (blue) and Nile Red (green) for 30 min and visualized by high-content imaging (40× magnification). Scale bars of the insets and the main images denote 20 and 100 μm, respectively. Bar graphs show the quantification of total lipid droplet areas following 48 h BDE-47 or OPE exposures. Data are shown as percentages relative to controls; values represent means ± SEM; $n = 6$–8. One-sample Holm-Bonferroni-corrected t tests were conducted to determine significant differences from controls (=100): $^{*}p < .05$, $^{**}p < .01$, and $^{***}p < .001$. For ease of visualization, only OPEs with significant findings at one or more treatment concentrations are shown, with concentrations ranged from 0.1 to 100 μM. Concentrations that induced > 30% cell death were excluded from the analyses.

shared similar heatmap patterns, which may indicate similar mode of actions; cell counts were negatively correlated with oxidative stress, mitochondrial parameters, lipid droplets, and positively correlated with lysosomal parameters. These phenotypes were also correlated with each other: for instance, a decrease in the number and intensity of lysosomes was associated with an increase in lipid droplets; reactive oxygen species (ROS) generation was positively associated with the number of mitochondria and the area of lipid droplets. Interestingly, this unique pattern of correlation matrix was only observed for several triaryl OPEs in the 2 steroidogenic cell lines (KGN and MA-10), but not in the C18-4 male germ cell line.

Potency Ranking

ToxPi approach. ToxPi analyses provide a complementary approach for use in visualizing and ranking the effects of chemicals on specific phenotypes. Chemicals were ranked based on their integrated effects on cell counts, Calcein intensity, oxidative stress, total and

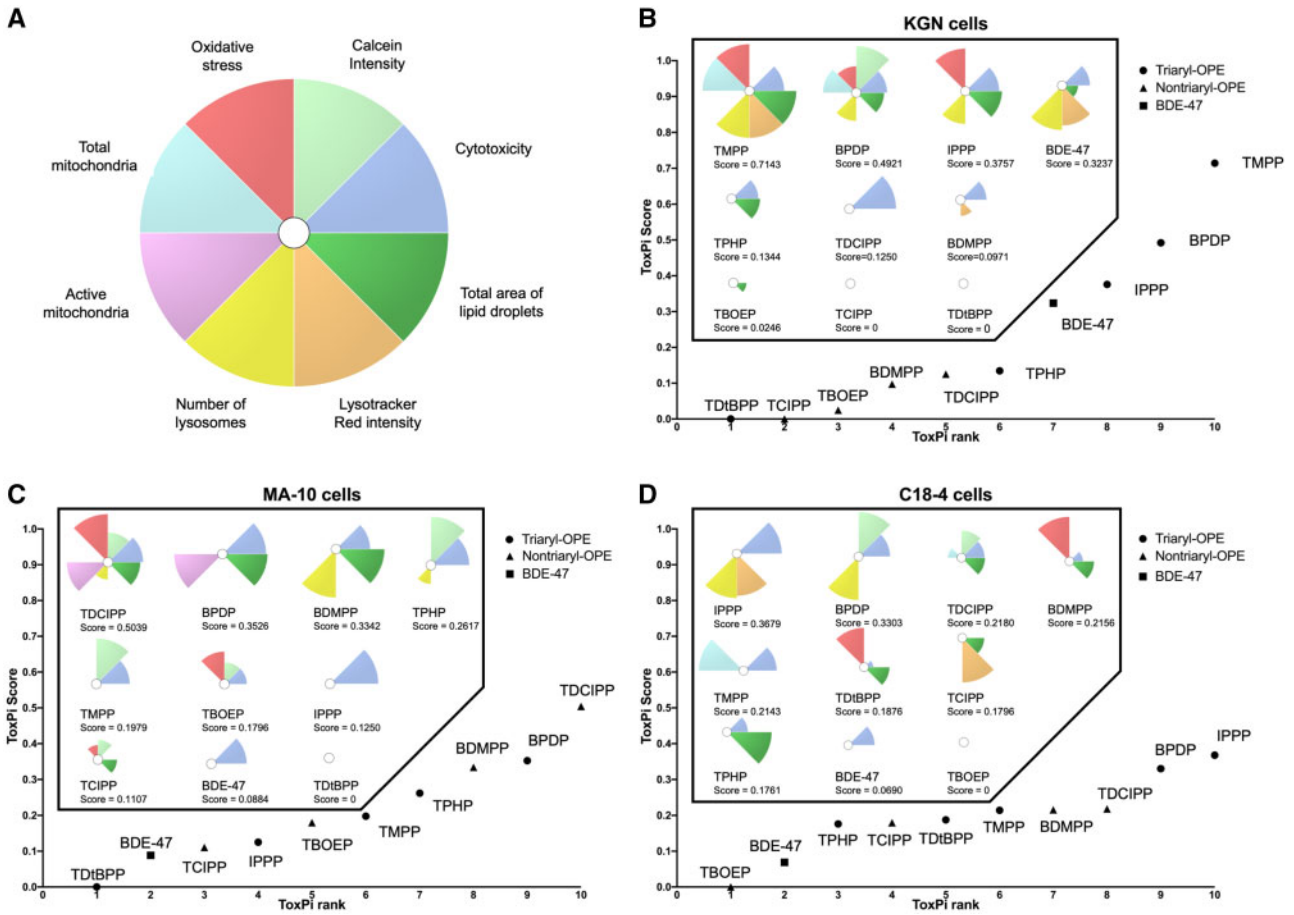

Figure 6. Toxicological Prioritization Index (ToxPi) analyses for chemical ranking. A, Eight endpoints were included in the analyses and their corresponding color preview for the ToxPi profiles. All endpoints were weighted equally. Ranking of chemicals based on their potencies in KGN cells (B), MA-10 cells (C), and C18-4 cells (D). Different symbols were used to indicate chemicals with specific structural characteristics: triaryl organophosphate esters (OPEs; circles), nontriaryl OPEs (triangles), 2,2′,4,4′-tetrabromodiphenyl ether (BDE-47; a square). Chemical-specific ToxPi profiles and ToxPi scores were shown in the box. Compound with the highest ToxPi score was ranked the highest (ie, the most potent).

active mitochondria, lysosome counts, Lysotracker Red intensity, and total lipid droplet areas (Figure 6A). ToxPi scores were generated accordingly as proxies of overall bioactivity of the test chemicals. Compounds with higher ToxPi scores are ranked higher and may be associated with a greater relative hazard potential. According to their ToxPi toxicity profiles, the cell line-specific ranking of chemicals was: TMPP > BPDP > IPPP > BDE-47 > TPHP > TDCIPP > BDMPP > TBOEP > TCIPP = TDtBPP, in KGN cells (Figure 6B); TDCIPP > BPDP > BDMPP > TPHP > TMPP > TBOEP > IPPP > TCIPP > BDE-47 > TDtBPP, in MA-10 cells (Figure 6C); IPPP > BPDP > TDCIPP > BDMPP > TMPP > TDtBPP > TCIPP > TPHP > BDE-47 > TBOEP, in C18-4 cells (Figure 6D). Interestingly, in KGN cells, the triaryl-OPEs were generally more potent than the nontriaryl OPEs regarding their ability to alter cell phenotypes. However, this distinction was not as evident in MA-10 and C18-4 cells. Further, hierarchical cluster analysis was done to group the chemicals based on their ToxPi profiles. The clustering dendrograms confirmed a clear separation between triaryl and nontriaryl OPEs in KGN cells, but not in the other 2 cell lines (Supplementary Figure 16).

Lowest observed BMC approach. Since changes in a single phenotype can indicate impaired cell functions, the test compounds were also ranked based on their lowest concentrations at which a 10% response in any of the endpoints was observed. Of note, the estimated BMC that fell outside the range of concentrations tested (0.001–100 μM) were excluded; in our dataset no BMC was lower than 0.001 μM.

In KGN cells, the rank order of chemical potency based on the lowest BMCs (regardless of endpoint) was: TMPP > IPPP > TDCIPP > BDE-47 > TPHP > BPDP > BDMPP > TBOEP > TCIPP = TDtBPP. Among all the chemicals tested, the most sensitive parameter tested, and thus, the lowest observed BMC, was for the effect of TMPP on lipid droplets (BMC_{10}: 1.2 μM; Figure 7A and Supplementary Table 3) in these cells.

In MA-10 and C18-4 cells, the only BMC value that was derived for BDE-47 was for cytotoxicity. In MA-10 cells, the rank order of chemical potency, based on the lowest BMCs (regardless of endpoint) was: BDMPP > TPHP > TMPP > IPPP > BPDP > TDCIPP > BDE-47 > TBOEP > TCIPP > TDtBPP (Figure 7B and Supplementary Table 3). The parameter affected by most chemicals in MA-10 cells was Calcein intensity. The lowest BMC was estimated for the effects of BDMPP on lysosome numbers (BMC_{10}: 0.1 μM).

In C18-4 cells, the rank order of chemical potency, based on the lowest BMCs (regardless of endpoint), was: TMPP > IPPP > BPDP > TPHP = TCIPP > BDMPP > TDtBPP > TDCIPP > BDE-47 > TBOEP (Figure 7C and Supplementary Table 3). The total area of lipid droplets was affected by many OPEs. The lowest BMC was derived from the TMPP-induced increase in total mitochondria (BMC_{10}: 1.4 μM).

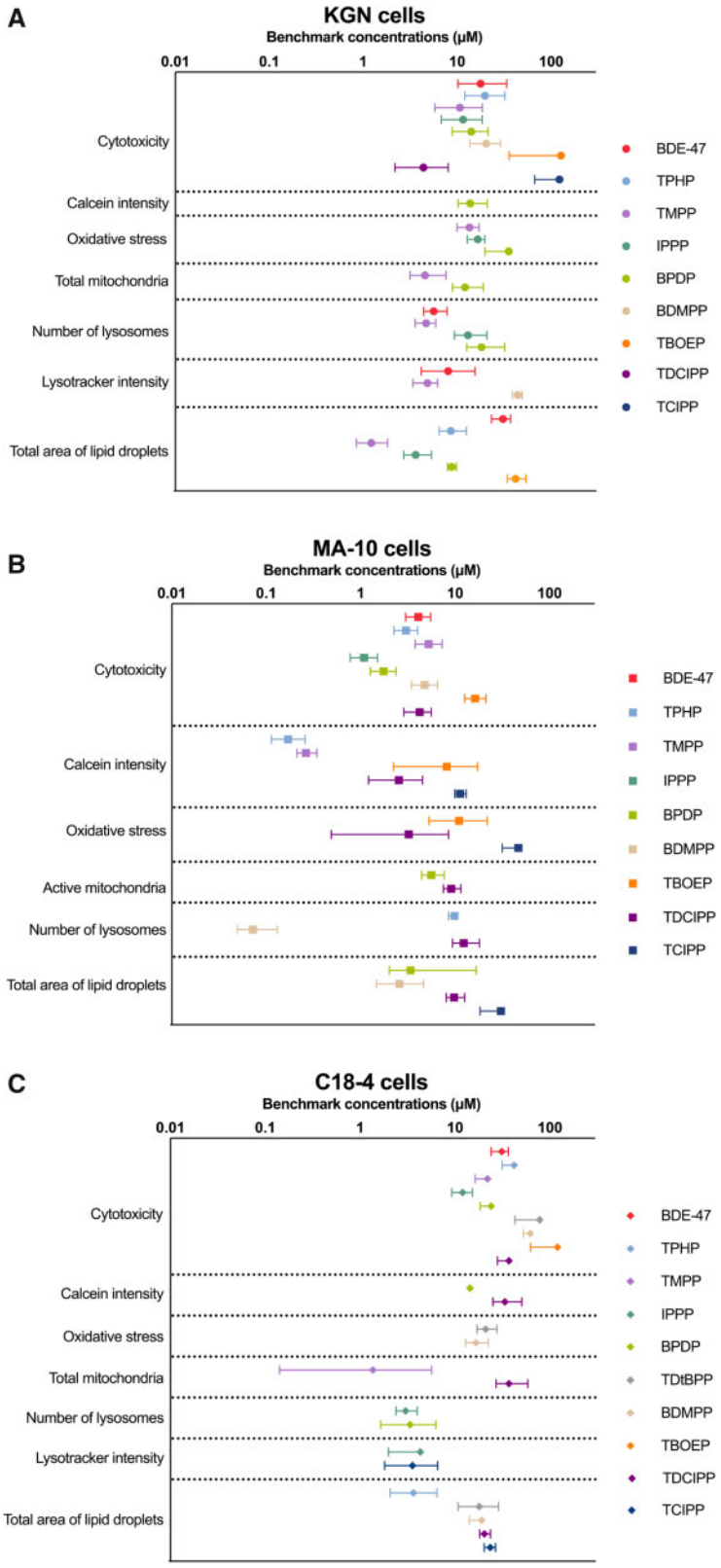

Figure 7. Benchmark concentration (μM) values of the test chemicals for specific endpoints in KGN cells (A), MA-10 cells (B), and C18-4 cells (C). The benchmark response (ie, a predetermined level of change from control) was set as 10%. Data points and error bars represent means ± upper and lower limits; $n = 6–8$. Some error bars cannot be shown because they were shorter than the size of symbols. Chemicals that are not on the graphs showed no effects on these endpoints or no significant benchmark model was generated.

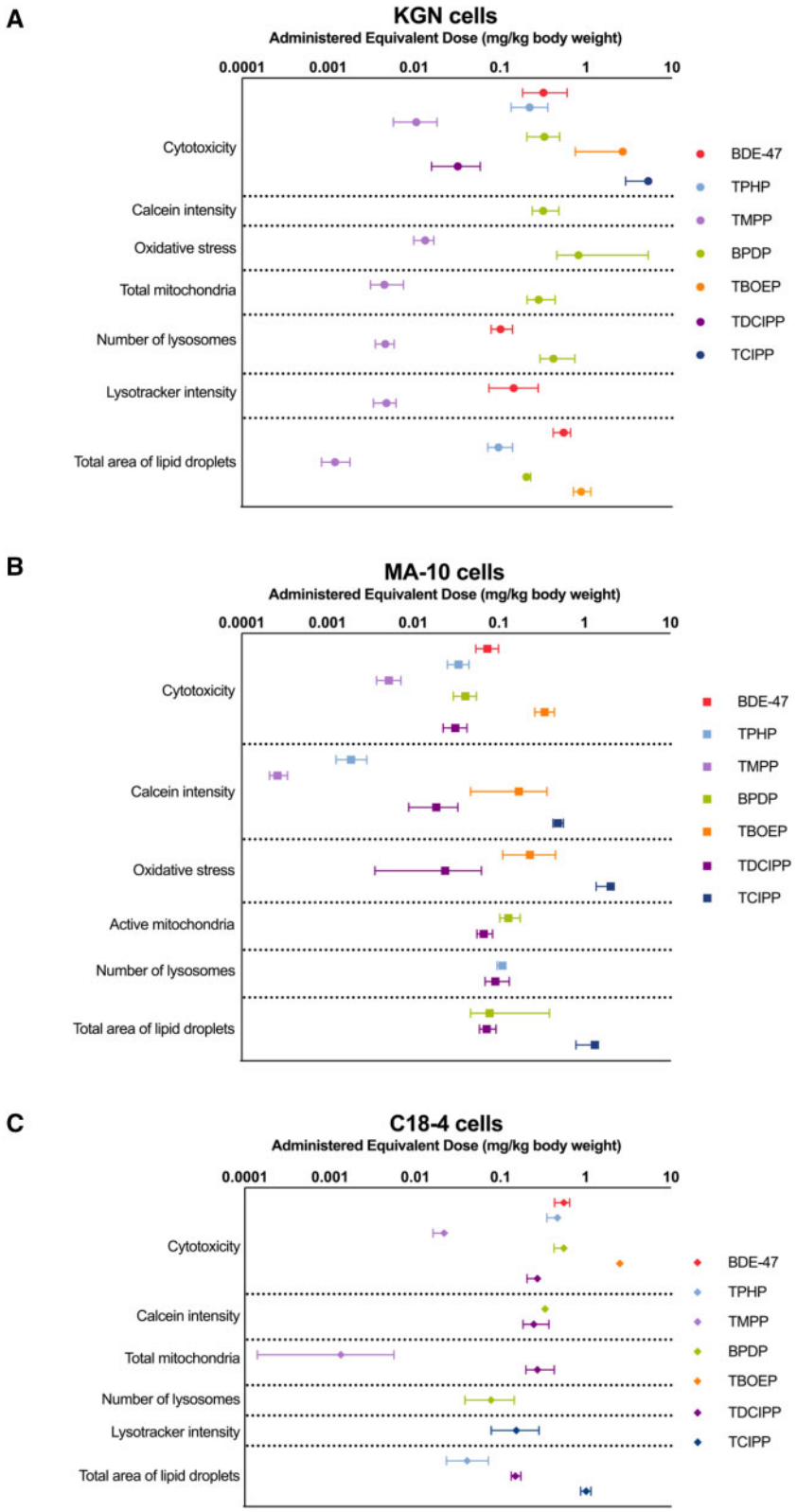

Figure 8. Administered equivalent dose (AED, mg/kg body weight) values of the test chemicals for specific endpoints in KGN cells (A), MA-10 cells (B), and C18-4 cells (C). AEDs were calculated by dividing the benchmark concentrations (μM) by steady-state concentrations (C_{ss}) of the chemicals. Data points and error bars represent means ± upper and lower limits; $n = 6–8$. Some error bars cannot be shown because they were shorter than the size of symbols. The AEDs of isopropylated triphenyl phosphate (IPPP), tris(2,4-di-*tert*-butylphenyl) phosphate (TDtBPP), and 2,4-bis(1,1-dimethylethyl)-phenol phosphate (BDMPP) are not calculated due to their high octanol-water partition coefficient (*LogKow*) and/or they are not applicable for the *in vitro* to *in vivo* extrapolation prediction algorithms.

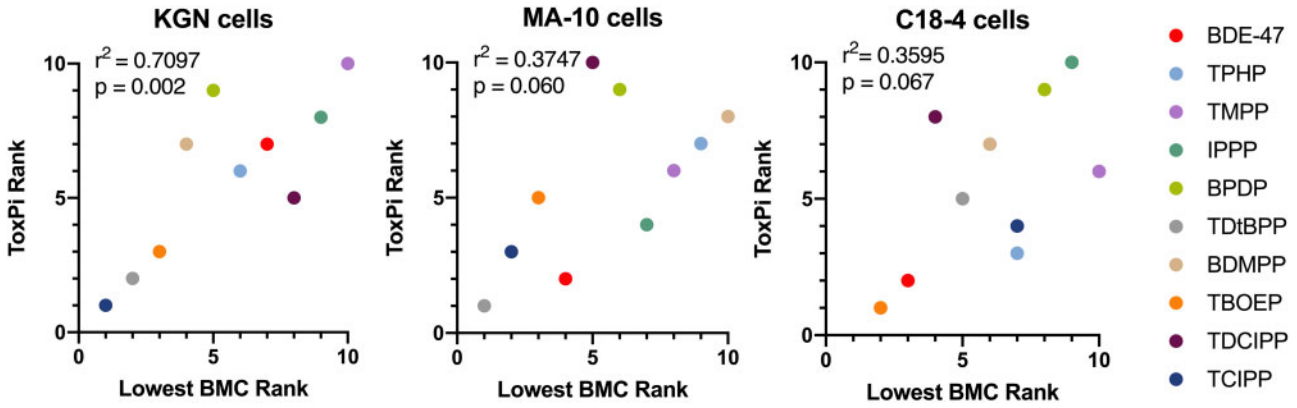

Figure 9. Correlations between the Toxicological Prioritization Index-based ranking and the lowest benchmark concentration-based ranking of chemical potencies in KGN, MA-10, and C18-4 cells. The squared Pearson's correlation coefficients (r^2) and statistical significance (p values) are indicated.

Notably, in many instances, alterations in cell phenotypes were observed at concentrations with low or no cytotoxicity, suggesting that these phenotypic parameters are a sensitive measure of insult. In general, the 3 cell lines responded very differently to OPE exposure. The MA-10 Leydig cell line was the most susceptible since phenotypic endpoints were affected at concentrations approximately 10 times lower than in KGN and C18-4 cells (Figure 7). In all 3 cell lines, many of the OPEs affected more phenotypic endpoints at lower concentrations than BDE-47; a few OPEs had little effect.

Lowest observed AED approach. AEDs (in mg/kg/day) were extrapolated from corresponding BMCs for each chemical to compare our phenotypic endpoints with doses that have been associated with effects after *in vivo* exposures (Figure 8 and Supplementary Table 4). The AEDs for IPPP, TDtBPP, and BDMPP were not modeled as they did not have available toxicokinetic data, had high *LogKow* values, and/or were outside the domain of applicability of the prediction model. In the 3 cell lines of interest, BDE-47 was estimated to affect cell phenotypes at doses ranging from 0.07 to 0.32 mg/kg/day. However, some OPEs were predicted to be bioactive in the lower microgram range. For example, the AED for TMPP was 0.3 μg/kg/day for its effect on Calcein intensity in MA-10 cells (Figure 8).

The rank order of chemicals using the lowest AEDs is very similar to that determined based on the BMCs. The most striking change was for TMPP, which had a modeled C_{ss} value that was 10- to 20-fold higher than the others. As a result, the AEDs for TMPP were generally 1–2 orders of magnitude lower than those for the other OPEs (Figure 8 and Supplementary Table 4). Thus, based on the lowest AEDs estimated for phenotypic endpoints in these experiments, TMPP was the most potent OPE tested.

Correlation analyses of rank orders determined with the ToxPi and lowest BMC approaches. Last, we compared the rank orders determined by the ToxPi and the lowest observed BMC approaches (Figure 9). In KGN cells, the ToxPi-based ranking was significantly correlated with the lowest BMC-based ranking (r^2 = 0.7097, p = .002), suggesting a high concordance between the rank orders. One of the outliers, TDCIPP, was highly cytotoxic to KGN cells in the absence of effects on cell phenotypes; this gave TDCIPP a high position in the lowest BMC rank and a lower position in the ToxPi rank. The other outlier, BPDP, had relatively high BMCs but affected a variety of phenotypes in KGN cells; therefore, it was ranked as number 5 by the lowest BMC but as number 9 using ToxPi.

Similarly, a trend of correlation was estimated in MA-10 (r^2 = 0.3747, p = .060) and C18-4 cells (r^2 = 0.3595, p = .067). Although the correlation was relatively weaker in these 2 cell lines, the rank orders shared some similarities at the 2 extremes. For example, TPHP, TMPP, BPDP, and BDMPP were ranked among the top 5 in MA-10 cells using both methods; TDtBPP and TCIPP were consistently ranked low. In C18-4 cells, IPPP and BPDP were potent and ranked in the top 3; BDE-47 and TBOEP were less active and ranked as the bottom 2.

In summary, we identified several OPEs that were consistently ranked highly in all 3 cell lines tested. TMPP exhibited high potency in all 3 cell lines. Other OPEs showed more cell-type-dependent activity: IPPP was highly active in KGN and C18-4 cells; BDMPP was ranked highest in MA-10 cells but was less active in the other 2 cell lines. TDtBPP, TBOEP, and TCIPP affected relative few parameters and had high BMCs and AEDs, suggesting that they may have fewer deleterious effects on cells of the reproductive system.

DISCUSSION

Few studies have compared the toxicity of brominated flame retardants and OPEs. Here, we showed that an isomeric mixture of TMPP was one of the most cytotoxic OPEs in KGN granulosa cells (IC_{50}: 49.7 μM; BMC_{10}: 19.8 μM; AED: 0.01 mg/kg/day). Our cytotoxicity data for the OPEs in MA-10 cells were similar (IC_{50}: 6.0–17.2 vs 10.3–27.5 μM) to those reported for 4 OPEs in a previous study by Schang *et al.* (2016). Cytotoxicity data for the effects of flame retardants in male germ cell models are scarce; in primary rat spermatogonial cells, TOCP was reported to decrease cell viability and induce autophagy (250–1000 μM) but only these high concentrations were tested (Liu *et al.*, 2015b). Overall, our data suggest that lipophilicity may be associated with cytotoxicity; OPEs with *LogKow* values (octanol/water partition coefficients) within a *LogKow* range from approximately 5 to 9 may be more cytotoxic than the others (Supplementary Table 2). A similar correlation between toxicity and *LogKow* was also observed for the effects of OPEs on zebrafish embryos (Du *et al.*, 2015), MA-10 Leydig cells (Schang *et al.*, 2016), Chinese hamster ovary (CHO-k1) cells (Huang *et al.*, 2017), and A549 adenocarcinoma cells (Yuan *et al.*, 2020).

Multiple cell phenotypes, including Calcein intensity, oxidative stress, mitochondria, lysosomes, and lipid droplets, were affected by OPE exposure. We observed significant increases in the intensity of Calcein staining in MA-10 and C18-4 cells following exposure to OPEs in the absence of an effect on cell

viability (Figure 2). Miles *et al.* (2015) observed greater Calcein fluorescence in rounded or nonadherent cells than in cells with spread morphology; however, we did not observe morphological changes at noncytotoxic concentrations. Increases in Calcein intensity may be due to inhibition of the efflux of Calcein-AM (Pasquier *et al.*, 2013) or be an indication of a change in intracellular oxidative state (Uggeri *et al.*, 2000). Calcein intensity increased concomitantly with an increase in MitoSox intensity (an indicator of superoxide production) in PBDE-exposed KGN cells (Lefevre et al., 2016b). Correlation analyses suggest moderate to strong correlations between cell counts, Calcein intensity, and oxidative stress (Supplementary Figure 15).

Several OPEs induced drastic increases in oxidative stress, as evidenced by CellROX intensity in KGN cells and MA-10 cells (Figs. 3A–D). In humans, an increase in ROS-producing granulosa cells was associated with poor pregnancy outcomes, such as impaired oocyte quality and decreased successful implantation (Jančar *et al.*, 2007; Lai *et al.*, 2018); further, exposure to OPEs was associated with increased expression of biomarkers for oxidative stress and DNA damage in pregnant women (Ingle *et al.*, 2020a,b; Yao *et al.*, 2021). In mouse ovarian tissues and primary granulosa cells, TOCP-induced oxidative stress, partially through decreasing the activities of 2 antioxidant enzymes, superoxide dismutase (SOD) and glutathione peroxidase (GPx; Hu *et al.*, 2019; Wang *et al.*, 2019; Yang *et al.*, 2020a,b). Similarly, in mouse Leydig TM3 cells, TOCP-reduced SOD and GPx activities, glutathione concentrations, and enhanced autophagic cell death (Liu *et al.*, 2016b). There is a need to investigate whether other OPEs increase oxidative stress via similar mechanisms. In contrast, C18-4 cells displayed low sensitivity to OPE-induced oxidative stress; exposure to TDtBPP and BDMPP decreased the overall oxidative levels in these cells (Figs. 3E and 3F). Of note, TDtBPP is one of the major degradation products of an antioxidant, Irgafos 168 (Yang *et al.*, 2016). Inadequate ROS may impair sperm functions, since ROS are important mediators of many physiological processes in sperm, including spermatogenesis and sperm capacitation (Agarwal *et al.*, 2014; Guerriero *et al.*, 2014).

We observed an increase in the total numbers of mitochondria in KGN cells and C18-4 cells following OPE exposure, while only active mitochondria were affected in MA-10 cells (Supplementary Figs. 1 and 2). Such effects may be indicative of a disruption in mitochondrial biogenesis, fusion, and fission, as well as in mitochondrial activity. OPEs have been reported previously to impair mitochondrial dynamics. In mouse hepatocyte AML12 cells, a few OPEs (including TPHP, TMPP, and TDCIPP) were found to increase the total area of mitochondria while reducing the numbers of branches in mitochondrial structure, suggesting mitochondrial fragmentation (Le *et al.*, 2021). These morphological changes were associated with increased local mitochondrial ROS production, depleted mitochondrial membrane potential, and disrupted mitochondrial respiration and ATP production (Le *et al.*, 2021). Further studies are needed to examine whether the increase in mitochondria that we observed is related to structural and functional changes. Similarly, exposure to several OPEs was reported to increase the number of mitochondria and decrease mitochondrial membrane potential in CHO-k1 and A549 cells (Huang *et al.*, 2017; Yuan *et al.*, 2020). The authors also demonstrated that OPEs increased ROS generation, cell cycle arrest, DNA damage, and mitochondria-mediated apoptosis (Huang *et al.*, 2017; Yuan *et al.*, 2020). We identified consistently high correlations among cytotoxicity, mitochondrial impairment, and oxidative stress for several OPEs in our datasets (Supplementary Figure 15).

Exposure to OPEs not only affected lysosome numbers in all 3 cell lines but also had the potential to disrupt the functions of lysosomal enzymes, as suggested by changes in staining intensity (Figure 4 and Supplementary Figure 3). Limited information is available on the effects of OPEs on lysosomes. However, OPEs were shown to induce autophagy in various types of cells (Liu *et al.*, 2015b, 2016b; Wang *et al.*, 2019; Yang *et al.*, 2020a,b). Moreover, in steroidogenic cells, lysosomes are involved in the process of cholesterol uptake from the circulation, which is an important source of cholesterol for steroid biosynthesis (Chang *et al.*, 2006). Indeed, OPEs were found to disrupt steroidogenesis in both *in vitro* and *in vivo* models (reviewed by Hales and Robaire, 2020; Wang *et al.*, 2021). Given the close links between lysosomes and these cellular functions, further investigations are needed to test whether they are related responses to OPE exposure.

After OPE exposure, drastic increases (up to 8-fold) were observed in the total area of lipid droplets in KGN cells; significant increases or decreases were also observed in MA-10 and C18-4 cells (Figure 5). In addition to storing energy to maintain cell homeostasis, lipid droplets in steroidogenic cells store cholesterol esters, thus serving as readily accessible reservoirs of cholesterol for steroidogenesis (Shen *et al.*, 2016). Schang *et al.* (2016) reported that several OPEs altered progesterone production in MA-10 cells (Schang *et al.*, 2016), and Liu *et al.* (2012) reported that OPEs affect estradiol production by H295R adrenal cells. In our datasets, a decrease in lysosome numbers was often concordant with an increase in lipid droplets (Supplementary Figure 15). In both mice and rats, OPEs have been reported to increase the levels of free cholesterol and cholesterol esters, cause vacuolation in ovarian and adrenal tissues and disrupt the balance of sex hormones (Carlton *et al.*, 1987; European Chemicals Agency [ECHA], 2010, 2021b,c; Hu *et al.*, 2019; Kinkead *et al.*, 1992; Latendresse *et al.*, 1993, 1994a, 1995; NTP [National Toxicology Program National Toxicology Program], 1994; Wang *et al.*, 2019). These increases are likely caused by a reduced activity (> 95% inhibition by OPE exposure) of neutral cholesterol ester hydrolase, an enzyme that deesterifies cholesterol esters and thus leads to their release from lipid droplets (Latendresse *et al.*, 1993). Moreover, lysosomes also play important roles in lipid metabolism (Singh *et al.*, 2009; Thelen and Zoncu, 2017); the decreases in lysosome numbers may contribute to lipid accumulation in cells. Other possible mechanisms are increased mobilization from the plasma membrane (a major source of cholesterol in MA-10 cells) (Freeman, 1989), increased *de novo* cholesterol synthesis, or disruption in cholesterol export.

Benchmark dose/concentration analysis has been used widely in priority setting and risk assessment for its advantages over the traditional no/lowest-observed-adverse-effect-level approach as it is less dependent on dose/concentration selection (Davis *et al.*, 2011; Health Canada, 2021). Herein, the derived BMCs are associated with a consistent response level and thus, enable meaningful comparisons across chemicals (ie, relative potencies) and across cell lines (ie, relative susceptibility). Notably, some effects of several OPEs were not taken into account in potency ranking because their BMCs were not available due to the poor fit of the models, for example, the BPDP-induced reduction in lysosome numbers in MA-10 cells. Therefore, this approach may underestimate the toxicity of some compounds.

In the existing studies on the *in vivo* reproductive toxicity of OPEs, the exposure doses used were often hundreds to thousands of mg/kg/day (reviewed by Hales and Robaire, 2020; Wang *et al.*, 2021). In this study, analyses of AEDs predict bioactivities

of OPEs at levels lower than those previously tested *in vivo*. According to the U.S. EPA, chronic or sub-chronic oral exposure of human populations to 0.02 mg/kg/day of TMPP or TDCIPP, or 0.01 mg/kg/day of TCIPP was estimated to have no appreciable risk of noncancer health effects during a lifetime (United States Environmental Protection Agency [U.S. EPA], 2021a). In our study, the AEDs derived for TDCIPP and TCIPP were close to the reference doses provided by the U.S. EPA. The lowest estimated AED was 0.3 μg/kg for daily exposure to TMPP.

The lowest BMC/AED approach ranks chemicals from a conservative perspective as alterations in a single endpoint can impact normal cell functions; this raises concerns if the chemical is active at low concentrations. A complementary analysis using the ToxPi tool provides a more complete picture of the overall bioactivities of chemicals. Overall, the 2 approaches reveal distinct rank orders; ToxPi analysis accounts for a number of affected endpoints and this may contribute to differences in potency ranking. Collectively, the 2 ranking approaches deliver important messages: one is more conservative, the other one is more comprehensive. Both approaches should be taken into consideration when assessing the risks associated with exposure to these chemicals.

CONCLUSIONS

In comparing the effects of 9 OPEs to those of a prominent brominated flame retardant, BDE-47, we found that the cell phenotypes were altered by several of the OPEs tested to a greater extent than by BDE-47, suggesting that these chemicals are more potent than the legacy compounds that they are replacing. It is noteworthy that these alterations in cell phenotypes were often observed at concentrations with low or no cytotoxicity, indicating that these chemicals may impair cell functions before apparent cell damage and death occur. The incorporation of high-content imaging, benchmark analyses, ToxPi ranking, and IVIVE is a high throughput and promising approach to compare chemical potencies within a family of chemicals and provides a path to identifying responsible replacements. Moreover, correlation analyses reveal potential cross-talking between multiple phenotypic endpoints and cell-type-specific effects induced by OPEs; a few triaryl OPEs showed a highly similar pattern of correlation heatmaps in KGN and MA-10 cells. This suggests that some OPEs that have similar physicochemical properties may share similar toxicity profiles. There is a need to test these chemicals in multiple cell types to fully assess their toxicity.

SUPPLEMENTARY DATA

Supplementary data are available at *Toxicological Sciences* online.

DECLARATION OF CONFLICTING INTERESTS

The authors declared no potential conflicts of interest with respect to the research, authorship, and/or publication of this article.

ACKNOWLEDGMENTS

We thank Dr Christopher Price and Dr Bruce Murphy (Université de Montréal, Montreal, Canada) and Dr Toshihiko Yanase (Fukuoka University, Japan) for providing and permitting the use of KGN cells, Dr Mario Ascoli (University of Iowa, USA) for providing MA-10 cells, and Dr Marie-Claude Hofmann (MD Anderson Cancer Center, University of Texas, USA) for providing C18-4 cells. We thank Dr Nicole Kleinstreuer from the NICEATM, Dr Michael G. Wade (Health Canada, Ottawa, Ontario, Canada), and Dr Heather M. Stapleton (Duke University, Durham, North Carolina, USA) for providing test chemicals. We thank Dr Nicolas Audet for his technical support in the use of the Operetta and the Columbus systems. Finally, we thank Dr Anne Marie Gannon and Dr Andy Nong for their helpful input during the article preparation.

FUNDING

Canadian Institutes of Health Research (CIHR) Institute for Population and Public Health team Grant (FRN No. IP3-150711); and McGill University. X.W. is the recipient of scholarships from McGill University and the Macau Government. B.F.H. and B.R. are James McGill Professors.

REFERENCES

Auerbach, S., Filer, D., Reif, D., Walker, V., Holloway, A. C., Schlezinger, J., Srinivasan, S., Svoboda, D., Judson, R., Bucher, J. R., *et al.* (2016). Prioritizing environmental chemicals for obesity and diabetes outcomes research: A screening approach using ToxCastTM high-throughput data. *Environ. Health Perspect.* **124**, 1141–1154.

Agarwal, A., Virk, G., Ong, C., and Plessis, S. S. and du, (2014). Effect of oxidative stress on male reproduction. *World J. Mens Health* **32**, 1–17.

Allais, A., Albert, O., Lefèvre, P. L. C., Wade, M. G., Hales, B. F., and Robaire, B. (2020). In utero and lactational exposure to flame retardants disrupts rat ovarian follicular development and advances puberty. *Toxicol. Sci.* **175**, 197–209.

Allen, J. G., Gale, S., Zoeller, T. R., Spengler, J. D., Birnbaum, L., and McNeely, E. (2016). PBDE flame retardants, thyroid disease, and menopausal status in U. S. women. *Environ. Health* **15**, 60.

Ascoli, M. (1981). Characterization of several clonal lines of cultured Leydig tumor cells: Gonadotropin receptors and steroidogenic responses. *Endocrinology* **108**, 88–95.

Blum, A., Behl, M., Birnbaum, L. S., Diamond, M. L., Phillips, A., Singla, V., Sipes, N. S., Stapleton, H. M., and Venier, M. (2019). Organophosphate ester flame retardants: Are they a regrettable substitution for polybrominated diphenyl ethers? *Environ. Sci. Tech. Lett.* **6**, 638–649.

Carignan, C. C., Mínguez-Alarcón, L., Butt, C. M., Williams, P. L., Meeker, J. D., Stapleton, H. M., Toth, T. L., Ford, J. B., Hauser, R., and Team, E. S. (2017). Urinary concentrations of organophosphate flame retardant metabolites and pregnancy outcomes among women undergoing in vitro fertilization. *Environ. Health Perspect.* **125**, 087018.

Carignan, C. C., Mínguez-Alarcón, L., Williams, P. L., Meeker, J. D., Stapleton, H. M., Butt, C. M., Toth, T. L., Ford, J. B., Hauser, R., and Team, E. S.; EARTH Study Team (2018). Paternal urinary concentrations of organophosphate flame retardant metabolites, fertility measures, and pregnancy outcomes among couples undergoing in vitro fertilization. *Environ. Int.* **111**, 232–238.

Carlton, B. D., Basaran, A. H., Mezza, L. E., and Smith, M. K. (1987). Examination of the reproductive effects of tricresyl

phosphate administered to Long-Evans rats. *Toxicology* **46**, 321–328.

Chang, T. Y., Chang, C. C. Y., Ohgami, N., and Yamauchi, Y. (2006). Cholesterol sensing, trafficking, and esterification. *Annu. Rev. Cell Dev. Biol.* **22**, 129–157.

Chapin, R. E., George, J. D., and Lamb, J. C. (1988). Reproductive toxicity of tricresyl phosphate in a continuous breeding protocol in Swiss (CD-1) mice. *Fund. Appl. Toxicol.* **10**, 344–354.

Chazotte, B. (2011). Labeling lysosomes in live cells with LysoTracker. *Cold Spring Harb. Protoc.* **2011**, pdb.prot5571.

Choi, G., Wang, Y. B., Sundaram, R., Chen, Z., Barr, D. B., Louis, G. M. B., and Smarr, M. M. (2019). Polybrominated diphenyl ethers and incident pregnancy loss: The LIFE Study. *Environ. Res.* **168**, 375–381.

Chokwe, T. B., Abafe, O. A., Mbelu, S. P., Okonkwo, J. O., and Sibali, L. L. (2020). A review of sources, fate, levels, toxicity, exposure and transformations of organophosphorus flame-retardants and plasticizers in the environment. *Emerg. Contam.* **6**, 345–366.

Darnerud, P. O. (2003). Toxic effects of brominated flame retardants in man and in wildlife. *Environ. Int.* **29**, 841–853.

Darnerud, P. O., Eriksen, G. S., Jóhannesson, T., Larsen, P. B., and Viluksela, M. (2001). Polybrominated diphenyl ethers: Occurrence, dietary exposure, and toxicology. *Environ. Health Perspect.* **109**, 49–68.

Davis, J. A., Gift, J. S., and Zhao, Q. J. (2011). Introduction to benchmark dose methods and U.S. EPA's benchmark dose software (BMDS) version 2.1.1. *Toxicol. Appl. Pharm.* **254**, 181–191.

Ding, J., Xu, Z., Huang, W., Feng, L., and Yang, F. (2016). Organophosphate ester flame retardants and plasticizers in human placenta in Eastern China. *Sci. Total Environ.* **554–555**, 211–217.

Du, Z., Wang, G., Gao, S., and Wang, Z. (2015). Aryl organophosphate flame retardants induced cardiotoxicity during zebrafish embryogenesis: By disturbing expression of the transcriptional regulators. *Aquat. Toxicol.* **161**, 25–32.

European Chemicals Agency (ECHA). (2010). Background document to the opinion of the committee for risk assessment on a proposal for harmonised classification and labelling of trixylyl phosphate. Available at: https://echa.europa.eu/documents/10162/fb3bd767-6bc3-fde3-9b3e-f2ab7a4e8d5e. Accessed June 26, 2021.

European Chemicals Agency (ECHA). (2021a). Registration dossier: 2-ethylhexyl diphenyl phosphate. Available at: https://echa.europa.eu/registration-dossier/-/registered-dossier/2152/7/9/1. Accessed June 26, 2021.

European Chemicals Agency (ECHA). (2021b). Registration dossier: Phenol, isopropylated, phosphate. Available at: https://echa.europa.eu/registration-dossier/-/registered-dossier/13333/7/9/1. Accessed June 26, 2021.

European Chemicals Agency (ECHA). (2021c) Dossier Evaluation status. Available at: https://echa.europa.eu/information-on-chemicals/dossier-evaluation-status. Accessed July 16, 2021.

Fan, X., Kubwabo, C., Rasmussen, P. E., and Wu, F. (2014). Simultaneous determination of thirteen organophosphate esters in settled indoor house dust and a comparison between two sampling techniques. *Sci. Total Environ.* **491–492**, 80–86.

Freeman, D. A. (1989). Plasma Membrane cholesterol: Removal and insertion into the membrane and utilization as substrate for steroidogenesis. *Endocrinology* **124**, 2527–2534.

Greaves, A. K., and Letcher, R. J. (2017). A review of organophosphate esters in the environment from biological effects to distribution and fate. *Bull. Environ. Contam. Toxicol.* **98**, 2–7.

Greenspan, P., Mayer, E. P., and Fowler, S. D. (1985). Nile red: A selective fluorescent stain for intracellular lipid droplets. *J. Cell Biol.* **100**, 965–973.

Guerriero, G., Trocchia, S., Abdel-Gawad, F. K., and Ciarcia, G. (2014). Roles of reactive oxygen species in the spermatogenesis regulation. *Front. Endocrinol.* **5**, 56.

Gulati, D. K., Barnes, L. H., Chapin, R. E., and Heindel, J. (1991). Final report on the reproductive toxicity of tris(2-chloroethyl)phosphate reproduction and fertility assessment in Swiss CD-1 mice when administered via gavage. PB92-129170 (as cited in: Provisional peer-reviewed toxicity values for tris(2-chloroethyl)phosphate), U.S. EPA 2009, pp. 11–16.

Hales, B. F., and Robaire, B. (2020). Effects of brominated and organophosphate ester flame retardants on male reproduction. *Andrology* **8**, 915–923.

Harley, K. G., Marks, A. R., Chevrier, J., Bradman, A., Sjödin, A., and Eskenazi, B. (2010). PBDE concentrations in women's serum and fecundability. *Environ. Health Perspect.* **118**, 699–704.

Health Canada. (2020) Report on Human Biomonitoring of Environmental Chemicals Pooled Samples. Available at: https://www.canada.ca/en/health-canada/services/environmental-workplace-health/environmental-contaminants/human-biomonitoring-environmental-chemicals/report-pooled-samples. html. Accessed January 26, 2022.

Health Canada. (2021) Science Approach Document: Bioactivity Exposure Ratio: Application in Priority Setting and Risk Assessment. Available at: https://www.canada.ca/en/environment-climate-change/services/evaluating-existing-substances/science-approach-document-bioactivity-exposure-ratio-application-priority-setting-risk-assessment.html. Accessed June 26, 2021.

Hoffman, K., Lorenzo, A., Butt, C. M., Hammel, S. C., Henderson, B. B., Roman, S. A., Scheri, R. P., Stapleton, H. M., and Sosa, J. A. (2017). Exposure to flame retardant chemicals and occurrence and severity of papillary thyroid cancer: A case-control study. *Environ. Int.* **107**, 235–242.

Hofmann, M.-C., Braydich-Stolle, L., Dettin, L., Johnson, E., and Dym, M. (2005). Immortalization of mouse germ line stem cells. *Stem Cells (Dayton, Ohio)* **23**, 200–210.

Hou, R., Xu, Y., and Wang, Z. (2016). Review of OPFRs in animals and humans: Absorption, bioaccumulation, metabolism, and internal exposure research. *Chemosphere* **153**, 78–90.

Hu, L., Peng, T., Huang, J., Su, T., Luo, R., Zheng, Y., Zhong, Z., Yu, P., Nie, K., and Zheng, L. (2019). Tri-ortho-cresyl phosphate (TOCP) induced ovarian failure in mice is related to the Hippo signaling pathway disruption. *Reprod. Toxicol.* **83**, 21–27.

Huang, C., Li, N., Yuan, S., Ji, X., Ma, M., Rao, K., and Wang, Z. (2017). Aryl- and alkyl-phosphorus-containing flame retardants induced mitochondrial impairment and cell death in Chinese hamster ovary (CHO-k1) cells. *Environ. Pollut.* **230**, 775–786.

Ingle, M. E., Mínguez-Alarcón, L., Carignan, C. C., Stapleton, H. M., Williams, P. L., Ford, J. B., Moravek, M. B., Hauser, R., Meeker, J. D., and Team, E. S.; EARTH Study Team (2020a). Exploring reproductive associations of serum polybrominated diphenyl ether and hydroxylated brominated diphenyl ether concentrations among women undergoing in vitro fertilization. *Hum. Reprod.* **35**, 1199–1210.

Ingle, M. E., Watkins, D., Rosario, Z., Vélez-Vega, C. M., Calafat, A. M., Ospina, M., Ferguson, K. K., Cordero, J. F., Alshawabkeh, A., and Meeker, J. D. (2020b). An exploratory analysis of

urinary organophosphate ester metabolites and oxidative stress among pregnant women in Puerto Rico. *Sci. Total Environ.* **703**, 134798.

Jančar, N., Kopitar, A. N., Ihan, A., Klun, I. V., and Bokal, E. V. (2007). Effect of apoptosis and reactive oxygen species production in human granulosa cells on oocyte fertilization and blastocyst development. *J. Assist. Reprod. Gen* **24**, 91–97.

Johnson, P. I., Altshul, L., Cramer, D. W., Missmer, S. A., Hauser, R., and Meeker, J. D. (2012). Serum and follicular fluid concentrations of polybrominated diphenyl ethers and in-vitro fertilization outcome. *Environ. Int.* **45**, 9–14.

Karmaus, A. L., Toole, C. M., Filer, D. L., Lewis, K. C., and Martin, M. T. (2016). High-throughput screening of chemical effects on steroidogenesis using H295R human adrenocortical carcinoma cells. *Toxicol. Sci.* **150**, 323–332.

Kinkead, E. R., Bunger, S. K., Wolfe, R. E., Brashear, W. T., and Latendresse, J. R. (1992). Dermal Absorption and Target Organ Toxicity of H19457C Hydraulic Fluid. In 1991 Toxic Hazards Research Unit Annual Technical Report, AL-TR-1992-0142, NMRI-92-97, Wright-Patterson Air Force Base, OH; Armstrong Laboratory and Naval Medical Research Institute, pp. 248–259.

Knight, P. G., and Glister, C. (2006). TGF-β superfamily members and ovarian follicle development. *Reproduction* **132**, 191–206.

Kojima, H., Takeuchi, S., Itoh, T., Iida, M., Kobayashi, S., and Yoshida, T. (2013). In vitro endocrine disruption potential of organophosphate flame retardants via human nuclear receptors. *Toxicology* **314**, 76–83.

Kubwabo, C., Kosarac, I., and Lalonde, K. (2013). Determination of selected perfluorinated compounds and polyfluoroalkyl phosphate surfactants in human milk. *Chemosphere* **91**, 771–777.

Kubwabo, C., Fan, X., Katuri, G. P., Habibagahi, A., and Rasmussen, P. E. (2021). Occurrence of aryl and alkyl-aryl phosphates in Canadian house dust. *Emerg. Contam.* **7**, 149–159.

Lai, Q., Xiang, W., Li, Q., Zhang, H., Li, Y., Zhu, G., Xiong, C., and Jin, L. (2018). Oxidative stress in granulosa cells contributes to poor oocyte quality and IVF-ET outcomes in women with polycystic ovary syndrome. *Front. Med.* **12**, 518–524.

Latendresse, J. R., Azhar, S., Brooks, C. L., and Capen, C. C. (1993). Pathogenesis of cholesteryl lipidosis of adrenocortical and ovarian interstitial cells in F344 rats caused by tricresyl phosphate and butylated triphenyl phosphate. *Toxicol. Appl. Pharm.* **122**, 281–289.

Latendresse, J. R., Brooks, C. L., and Capen, C. C. (1994a). Pathologic effects of butylated triphenyl phosphate-based hydraulic fluid and tricresyl phosphate on the adrenal gland, ovary, and testis in the fischer-344 rat. *Toxicol. Pathol.* **22**, 341–352.

Latendresse, J. R., Brooks, C. L., and Capen, C. C. (1995). Toxic effects of butylated triphenyl phosphate-based hydraulic fluid and tricresyl phosphate in female F344 rats. *Vet. Pathol.* **32**, 394–402.

Latendresse, J. R., Brooks, C. L., Flemming, C. D., and Capen, C. C. (1994b). Reproductive Toxicity of Butylated Triphenyl Phosphate and Tricresyl Phosphate Fluids in F344 Rats. *Fund Appl Toxicol* **22**, 392–399.

Le, Y., Shen, H., Yang, Z., Lu, D., and Wang, C. (2021). Comprehensive analysis of organophosphorus flame retardant-induced mitochondrial abnormalities: Potential role in lipid accumulation. *Environ. Pollut.* **274**, 116541.

Lefèvre, P. L. C., Berger, R. G., Ernest, S. R., Gaertner, D. W., Rawn, D. F., Wade, M. G., Robaire, B., and Hales, B. F. (2016a). Exposure of female rats to an environmentally relevant mixture of brominated flame retardants targets the ovary, affecting folliculogenesis and steroidogenesis. *Biol. Rreprod.* **94**, 9.

Lefèvre, P. L. C., Nardelli, T. C., Son, W. Y., Sadler, A. R., Rawn, D. F. K., Goodyer, C., Robaire, B., and Hales, B. F. (2021). Polybrominated diphenyl ethers in human follicular fluid dysregulate mural and cumulus granulosa cell gene expression. *Endocrinology* **162**, bqab003.

Lefevre, P. L. C., Wade, M. G., Goodyer, C., Hales, B. F., and Robaire, B. (2016b). A mixture reflecting polybrominated diphenyl ether (PBDE) profiles detected in human follicular fluid significantly affects steroidogenesis and induces oxidative stress in a female human granulosa cell line. *Endocrinology* **157**, 2698–2711.

Leonetti, C., Butt, C. M., Hoffman, K., Hammel, S. C., Miranda, M. L., and Stapleton, H. M. (2016). Brominated flame retardants in placental tissues: Associations with infant sex and thyroid hormone endpoints. *Environ. Health* **15**, 113.

Liu, L. Y., He, K., Hites, R. A., and Salamova, A. (2016a). Hair and nails as noninvasive biomarkers of human exposure to brominated and organophosphate flame retardants. *Environ. Sci. Technol.* **50**, 3065–3073.

Liu, L. Y., Salamova, A., He, K., and Hites, R. A. (2015a). Analysis of polybrominated diphenyl ethers and emerging halogenated and organophosphate flame retardants in human hair and nails. *J. Chromatogr. A* **1406**, 251–257.

Liu, M. L., Wang, J. L., Wei, J., Xu, L. L., Yu, M., Liu, X. M., Ruan, W. L., and Chen, J. X. (2015b). Tri-ortho-cresyl phosphate induces autophagy of rat spermatogonial stem cells. *Reproduction* **149**, 163–170.

Liu, X., Ji, K., and Choi, K. (2012). Endocrine disruption potentials of organophosphate flame retardants and related mechanisms in H295R and MVLN cell lines and in zebrafish. *Aquat. Toxicol.* **114**, 173–181.

Liu, X., Xu, L., Shen, J., Wang, J., Ruan, W., Yu, M., and Chen, J. (2016b). Involvement of oxidative stress in tri-ortho–cresyl phosphate-induced autophagy of mouse Leydig TM3 cells in vitro. *Reprod. Biol. Endocrinol* **14**, 30.

Marvel, S. W., To, K., Grimm, F. A., Wright, F. A., Rusyn, I., and Reif, D. M. (2018). ToxPi Graphical User Interface 2.0: Dynamic exploration, visualization, and sharing of integrated data models. *BMC Bioinformatics* **19**, 80.

Miles, F., Lynch, J., and Sikes, R. (2015). Cell-based assays using Calcein acetoxymethyl ester show variation in fluorescence with treatment conditions. *J. Biol. Methods* **2**, e29.

Nishi, Y., Yanase, T., Mu, Y., Oba, K., Ichino, I., Saito, M., Nomura, M., Mukasa, C., Okabe, T., Goto, K., *et al.* (2001). Establishment and characterization of a steroidogenic human granulosa-like tumor cell line, KGN, that expresses functional follicle-stimulating hormone receptor. *Endocrinology* **142**, 437–445.

NTP (National Toxicology Program). (1994) Toxicology And Carcinogenesis Studies of Tricresyl Phosphate (CAS No. 1330-78-5) in F334/N Rats and B6C3F1 Mice (Gavage and Feed Studies). U.S. Department of Health and Human Services, Public Health Service, National Institutes of Health, Research Triangle Park, NC, USA.

Pasquier, J., Rioult, D., Abu-Kaoud, N., Marie, S., Rafii, A., Guerrouahen, B. S., and Le Foll, F. (2013). P-glycoprotein-activity measurements in multidrug resistant cell lines: Single-cell versus single-well population fluorescence methods. *Biomed. Res. Int.* **2013**, 676845.

Peng, B., Yu, Z. M., Wu, C. C., Liu, L. Y., Zeng, L., and Zeng, E. Y. (2020). Polybrominated diphenyl ethers and organophosphate

esters flame retardants in play mats from China and the exposure risks for children. *Environ. Int.* **135**, 105348.

Percy, Z., Guardia, M. J. L., Xu, Y., Hale, R. C., Dietrich, K. N., Lanphear, B. P., Yolton, K., Vuong, A. M., Cecil, K. M., Braun, J. M., *et al.* (2020). Concentrations and loadings of organophosphate and replacement brominated flame retardants in house dust from the home study during the PBDE phase-out. *Chemosphere* **239**, 124701.

Rahman, F., Langford, K. H., Scrimshaw, M. D., and Lester, J. N. (2001). Polybrominated diphenyl ether (PBDE) flame retardants. *Sci. Total Environ.* **275**, 1–17.

Rajkumar, A., Luu, T., Beal, M. A., Barton-Maclaren, T. S., Robaire, B., and Hales, B. F. (2021). Elucidation of the effects of bisphenol A and structural analogs on germ and steroidogenic cells using single cell high-content imaging. *Toxicol. Sci.* **180**, 224–238.

Ruis, M. T., Rock, K. D., Hall, S. M., Horman, B., Patisaul, H. B., and Stapleton, H. M. (2019). PBDEs concentrate in the fetal portion of the placenta: Implications for thyroid hormone dysregulation. *Endocrinology* **160**, 2748–2758.

Schang, G., Robaire, B., and Hales, B. F. (2016). Organophosphate flame retardants act as endocrine-disrupting chemicals in MA-10 mouse tumor leydig cells. *Toxicol. Sci.* **150**, 499–509.

Shen, W. J., Azhar, S., and Kraemer, F. B. (2016). Lipid droplets and steroidogenic cells. *Exp. Cell Res.* **340**, 209–214.

Sjödin, A., Jones, R. S., Wong, L.-Y., Caudill, S. P., and Calafat, A. M. (2019). Polybrominated diphenyl ethers and biphenyl in serum: time trend study from the national health and nutrition examination survey for years 2005/06 through 2013/14. *Environ. Sci. Technol.* **53**, 6018–6024.

Siddique, S., Harris, S. A., Kosarac, I., Latifovic, L., and Kubwabo, C. (2020). Urinary metabolites of organophosphate esters in women and its relationship with serum lipids: An exploratory analysis. *Environ. Pollut.* **263**, 114110.

Singh, R., Kaushik, S., Wang, Y., Xiang, Y., Novak, I., Komatsu, M., Tanaka, K., Cuervo, A. M., and Czaja, M. J. (2009). Autophagy regulates lipid metabolism. *Nature* **458**, 1131–1135.

Smith, L. B., and Walker, W. H. (2014). The regulation of spermatogenesis by androgens. *Semin. Cell Dev. Biol.* **30**, 2–13.

Stapleton, H. M., Eagle, S., Sjödin, A., and Webster, T. F. (2012). Serum PBDEs in a North Carolina Toddler Cohort: Associations with handwipes, house dust, and socioeconomic variables. *Environ. Health Perspect.* **120**, 1049–1054.

The Government of Canada. (2021). Summary of flame retardant assessments and management conducted under the Canadian Environmental Protection Act, 1999. Available at: https://www.canada.ca/en/environment-climate-change/services/evaluating-existing-substances/summary-flame-retardant-assessments-management-conducted-cepa.html. Accessed May, 2021.

Thelen, A. M., and Zoncu, R. (2017). Emerging roles for the lysosome in lipid metabolism. *Trends Cell Biol.* **27**, 833–850.

Tung, E. W. Y., Kawata, A., Rigden, M., Bowers, W. J., Caldwell, D., Holloway, A. C., Robaire, B., Hales, B. F., and Wade, M. G. (2017). Gestational and lactational exposure to an environmentally-relevant mixture of brominated flame retardants: Effects on neurodevelopment and metabolism. *Birth Defects Res.* **109**, 497–512.

Tung, E. W. Y., Yan, H., Lefèvre, P. L. C., Berger, R. G., Rawn, D. F. K., Gaertner, D. W., Kawata, A., Rigden, M., Robaire, B., Hales, B. F., *et al.* (2016). Gestational and early postnatal exposure to an environmentally relevant mixture of brominated flame retardants: General toxicity and skeletal variations. *Birth Defects Res. B Dev. Reprod. Toxicol.* **107**, 157–168.

United States Environmental Protection Agency (U.S. EPA). (2012). Benchmark Dose Technical Guidance. Washington, DC 20460: Risk Assessment Forum, U.S. EPA Report EPA/100/R-12/001. Available at: https://www.epa.gov/risk/benchmark-dose-technical-guidance. Accessed June 26, 2021.

United States Environmental Protection Agency (U.S. EPA). (2014). Final Report: An Alternatives Assessment for the Flame Retardant Decabromodiphenyl Ether (DecaBDE). Available at: https://www.epa.gov/sites/default/files/2014-05/documents/decabde_final.pdf. Accessed July 16, 2021.

United States Environmental Protection Agency (U.S. EPA). (2021a). Regional Screening Levels (RSLs) - Generic Tables (as of May 2021). Available at: https://www.epa.gov/risk/regional-screening-levels-rsls-generic-tables. Accessed July 16, 2021.

United States Environmental Protection Agency (U.S. EPA). (2021b), Tox21/ToxCast database, CompTox Chemicals Dashboard. Available at: https://comptox.epa.gov/dashboard/. Accessed July 10, 2021.

Uggeri, J., Gatti, R., Belletti, S., Scandroglio, R., Corradini, R., Rotoli, B. M., and Orlandini, G. (2000). Calcein-AM is a detector of intracellular oxidative activity. *Histochem. Cell Biol.* **122**, 499–505.

van der Veen, I., and van der de Boer, J. (2012). Phosphorus flame retardants: Properties, production, environmental occurrence, toxicity and analysis. *Chemosphere* **88**, 1119–1153.

Wang, J., Ruan, W., Huang, B., Shao, S., Yang, D., Liu, M., Zeng, L., Wei, J., and Chen, J. (2019). Tri-*ortho*-cresyl phosphate induces autophagy of mouse ovarian granulosa cells. *Reproduction* **158**, 61–69.

Wang, X., Hales, B. F., and Robaire, B. (2021). Effects of flame retardants on ovarian function. *Reprod. Toxicol.* **102**, 10–23.

Yang, B., Wang, X., Ma, Y., Yan, L., Ren, Y., Yu, D., Qiao, B., Shen, X., Liu, H., Zhang, D., *et al.* (2020a). Tri-*ortho*-cresyl phosphate (TOCP)-induced reproductive toxicity involved in placental apoptosis, autophagy and oxidative stress in pregnant mice. *Environ. Toxicol.* **35**, 97–107.

Yang, S., Shao, S., Huang, B., Yang, D., Zeng, L., Gan, Y., Long, D., Chen, J., and Wang, J. (2020b). Tea polyphenols alleviate tri-*ortho*-cresyl phosphate-induced autophagy of mouse ovarian granulosa cells. *Environ. Toxicol.* **35**, 478–486.

Yang, Y., Hu, C., Zhong, H., Chen, X., Chen, R., and Yam, K. L. (2016). Effects of ultraviolet (UV) on degradation of irgafos 168 and migration of its degradation products from polypropylene films. *J. Agric. Food Chem.* **64**, 7866–7873.

Yao, Y., Li, M., Pan, L., Duan, Y., Duan, X., Li, Y., and Sun, H. (2021). Exposure to organophosphate ester flame retardants and plasticizers during pregnancy: Thyroid endocrine disruption and mediation role of oxidative stress. *Environ. Int.* **146**, 106215.

Yuan, S., Zhu, K., Ma, M., Zhu, X., Rao, K., and Wang, Z. (2020). In vitro oxidative stress, mitochondrial impairment and G1 phase cell cycle arrest induced by alkyl-phosphorus-containing flame retardants. *Chemosphere* **248**, 126026.